



INQUA Focus Group on Paleoseismology and Active Tectonics



paleoseismicity.org

TRAINING SESSION IN PALEOSEISMOLOGY

Student Training Course for the
Workshop on Paleoseismology, Active Tectonics, and
Archaeoseismology

Focus Group on Paleoseismology and Active Tectonics
INQUA Terrestrial Processes Commission
02-JUNE-2016



Field traverse along the Villa Grove Fault Zone

Edited by J.P. McCalpin

Trip Leaders: James P. McCalpin, Christoph Gruetzner, Petra Stepancikova,
Jakub Stemberk, Ed Nissen, Ramon Arrowsmith, Alan R. Nelson

Guidebook 11
Crestone Science Center
P.O. Box 837
Crestone, CO 81131 USA
14-MAY-2016
ISBN: 978-0-9974355-0-4



INQUA Focus Group on Paleoseismology and Active Tectonics



paleoseismicity.org

TRAINING SESSION IN PALEOSEISMOLOGY

EDITOR: James P. McCalpin, GEO-HAZ Consulting & Crestone Science Center, Box 837, Crestone, CO 81131; phone (719) 256-5227, cell phone (719) 588-4279, mccalpin@geohaz.com

Trip Sponsor:



Crestone Science Center, Inc.

*Education and Research
in the Earth Sciences*

TABLE OF CONTENTS

ROUTE MAP	4
INTRODUCTION and Acknowledgements	3
1-Locating Fault Traces; Unmanned Aerial Vehicles (UAVs) vs Lidar vs Stereo Aerial Photographs.....	6
2-Geophysics; Locating buried structures.....	7
3-Paleoseismic Trench Logging Techniques; Manual vs 2D Photomosaic vs 3D Structure from Motion.....	21
4-The Importance of Soil Stratigraphy and Dating in Paleoseismology	27
REFERENCES	33



INTRODUCTION

Student Training sessions will be held all afternoon Thursday, June 2, mostly at field sites on the Villa Grove Fault Zone north of Crestone (Fig. 1). THESE TRAINING SESSIONS ARE OPEN TO STUDENTS, EARLY CAREER RESEARCHERS, AND EXPERIENCED PALEOSEISMOLOGISTS WHO WANT TO LEARN MORE ABOUT FIELD TECHNIQUES. E.G., ANY PATA DAYS ATTENDEES. See the List of Training Activities, below.

PATA attendees who do not wish to attend the Training Sessions on Thursday afternoon will have a choice of several other activities;

1-all afternoon bus trip to Great Sand Dunes National Park; play in Medano Creek, unique surging stream; hike the high dune (600 ft high); look at Holo fault scarps and range-front landslide formed by backsliding on a valleyward-dipping old thrust fault

2- in Crestone; 2-3 hour hike to the crest of terminal moraine complex of Willow Creek; drop down into old lake bed, now a meadow; lakebed was cored in 1979 with C14 dates on postglacial sequence of mud vs peat beds

3-in Crestone; Western horseback trail ride at the Baca Grande Stables

4-on-your-own nudist experience at Valley View Hot Springs

5-stop at Recreational Marijuana store in Moffat, 12 mi W of Crestone

List of Training Activities

1-Locating Fault Traces; Unmanned Aerial Vehicles (UAVs) vs Lidar vs Stereo Aerial Photographs

2-Geophysics; Locating buried structures

3-Paleoseismic Trench Logging Techniques; Manual vs 2D Photomosaic vs 3D Structure from Motion

4-The Importance of Soil Stratigraphy and Dating in Paleoseismology

Location of Training Activities

Most training activities will take place on the Villa Grove Fault Zone (VGFZ), 30-40 km north of Crestone (see Fig. 1). Fault scarps of the VGFZ are smaller and more accessible than those of the range-front Sangre de Cristo Fault Zone (SCFZ), making them a bit easier to study. In addition, they lie on the grassy valley floor, so are not obscured by trees. This makes imaging the scarps via UAVs easier, as well as scarp profiling and trenching. We will take advantage of well-preserved fault scarps and a 3 m-deep trench to describe techniques for collecting paleoseismic data from fault traces (On-Fault studies). For more information about the VGFZ, go to: http://geohazards.usgs.gov/cfusion/qfault/show_report_AB.cfm?fault_id=2319§ion_id=

Acknowledgments: We thank the Orient Land Trust for permitting access to the paleoseismic teaching trench, and to John Eiseman for access to the scarps at Major Creek.



INQUA Focus Group on Paleoseismology and Active Tectonics



paleoseismicity.org

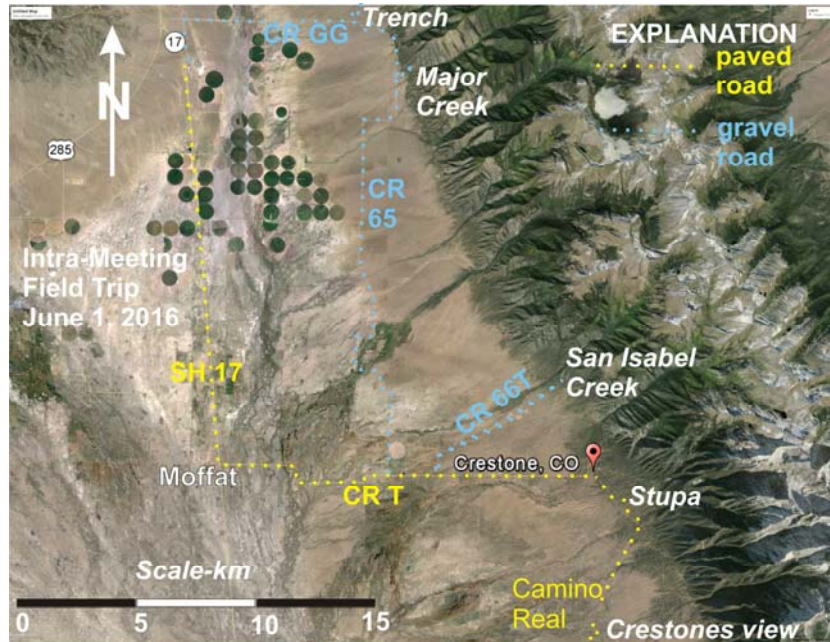


Fig. 1a. Route map of the Intra-Meeting field trip. The Training Sessions will follow a similar route. Paved roads (yellow dotted lines) and unpaved roads (blue dotted lines) in the northern San Luis Valley.

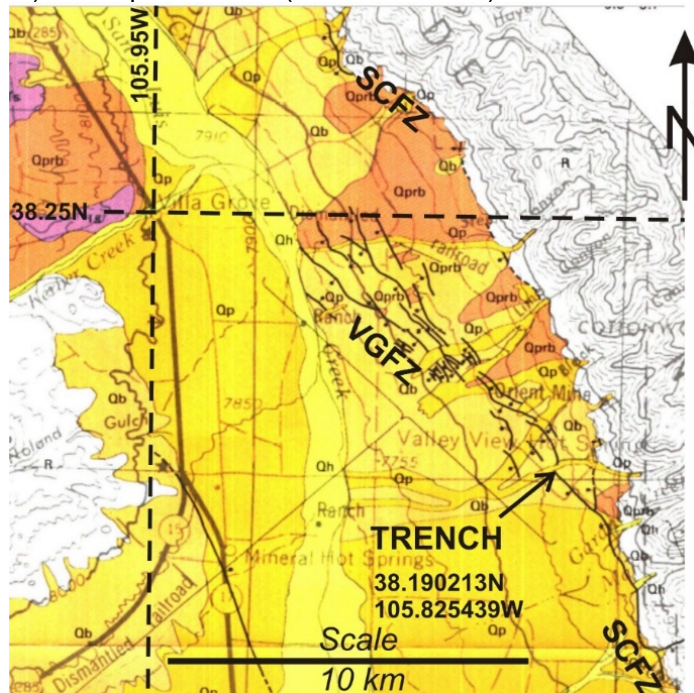


Fig. 1b. Map of the Villa Grove Fault Zone (VGFZ), a splay fault swarm on the valley floor where training sessions will be held. Colored polygons show different ages of alluvial deposits (darker yellow, Qp, Pinedale age, ~15-35 ka, MIS Stage 2; lighter yellow, Qb, Bull Lake age, ~150 ka, MIS Stage 6; red, Qprb, pre-Bull Lake age, >400 ka). Bedrock areas are uncolored; SCFZ marks the range-front Sangre de Cristo fault zone. From Colman et al., 1985, USGS Map I-1594.



ON-FAULT INVESTIGATIONS

On-Fault investigations generally follow the flow chart shown below (Fig. 2). Training Sessions will follow this stepwise approach, starting with locating the fault traces.

Flow Chart for Performing Paleoseismic Trenching Studies

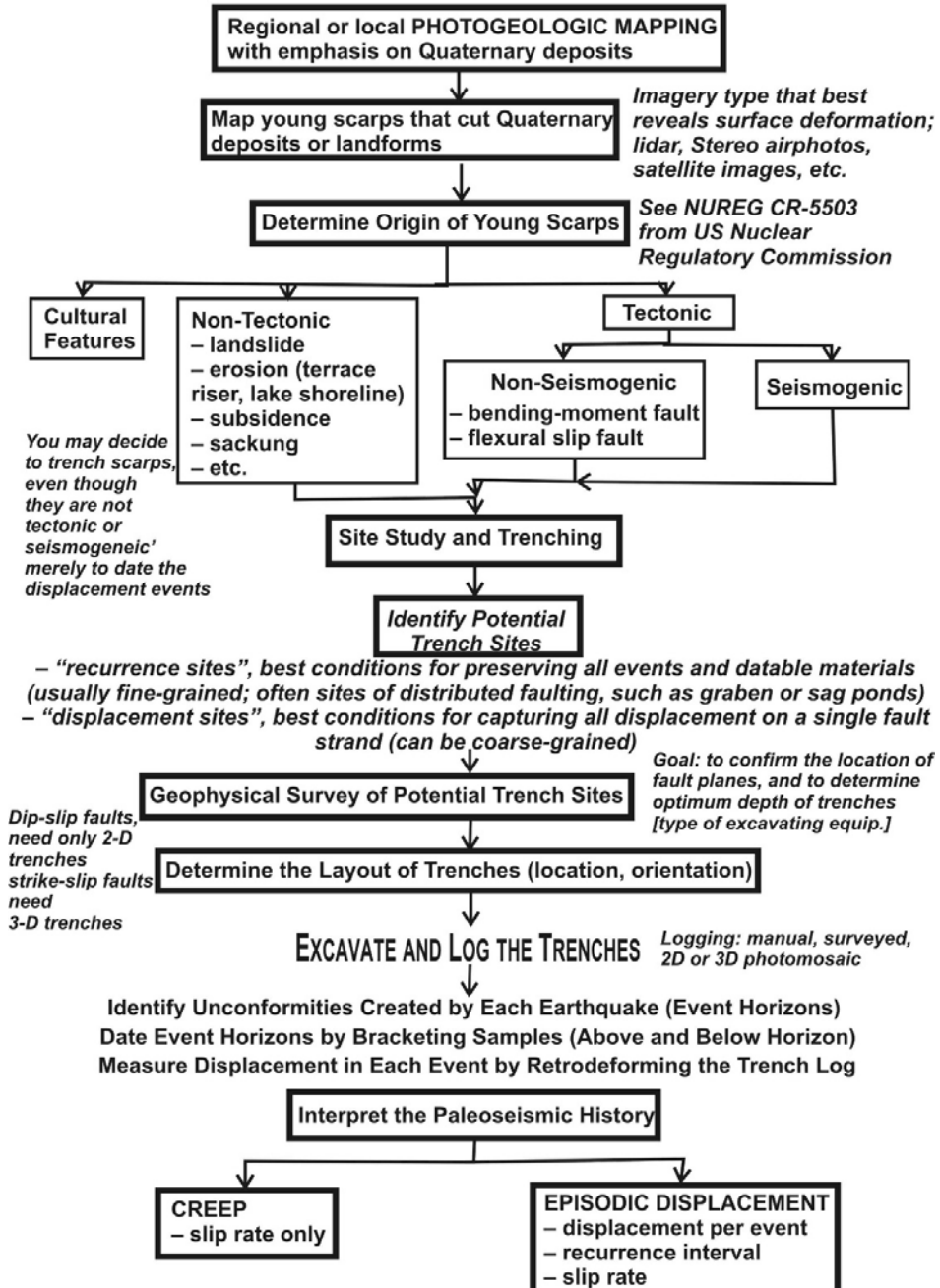


Fig. 2. Generalized flow chart for performing on-fault paleoseismic studies. Updated from McCalpin, 2009, Paleoseismology, Academic Press, 2nd Edition.



INQUA Focus Group on Paleoseismology and Active Tectonics



paleoseismicity.org

1-LOCATING FAULT TRACES; UNMANNED AERIAL VEHICLES (UAVS) VS LIDAR VS STEREO AERIAL PHOTOGRAPHS

INSTRUCTORS:

Dr. Ed Nissen(Department of Geophysics, Colorado School of Mines)

Dr. Ramon Arrowsmith (Arizona State University; Active Tectonics, Quantitative Structural Geology and Geomorphology Group)

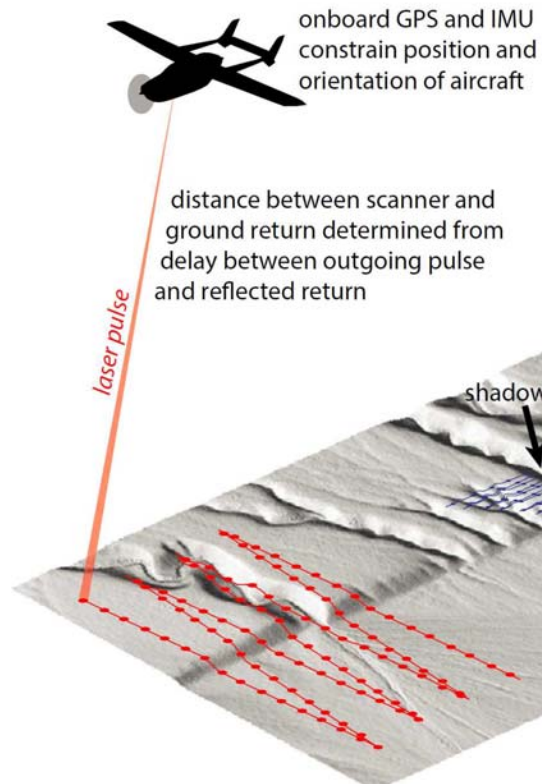
EQUIPMENT:

LESSON PLAN:

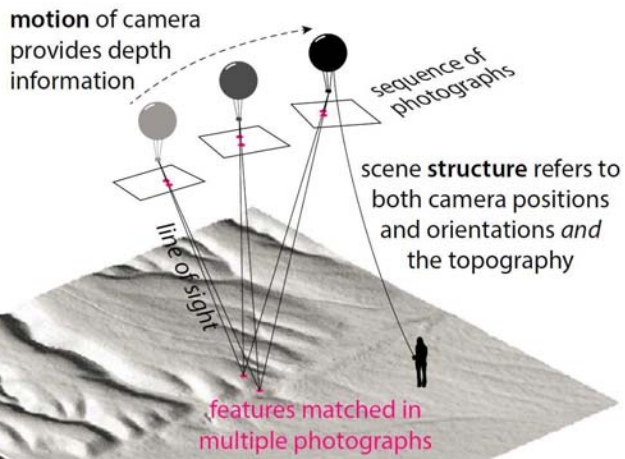
In the past 10 years major advances have been made in remote sensing methods to locating fault traces and measuring coseismic offsets. **Dr. Ed Nissen** will demonstrate use of unmanned aerial vehicles (balloons and drones) to collect local topographic information, and Structure-from-Motion methods of creating Digital Elevation Models (DEMs).

Dr. Ramon Arrowsmith will describe high resolution topographic data gathered by lidar and its use in locating and characterizing fault traces. The entire Colorado portion of the Rio Grande Rift is covered by 1-m lidar DEMs, which will be given to participants on a USB stick.

A Airborne LiDAR



C Structure from Motion



B Terrestrial LiDAR

lines show track of scan across ground
circles show actual ground return footprints



2-GEOPHYSICS; LOCATING BURIED STRUCTURES

INSTRUCTORS:

Dr. Christoph Gruetzner (Department of Earth Sciences, University of Cambridge, UK)
Dr. Petra Štěpančíková (Institute of Rock Structure and Mechanics, Academy of Sciences of the Czech Republic)
Dr. Jakub Stemberk (Institute of Rock Structure and Mechanics, Academy of Sciences of the Czech Republic)

EQUIPMENT:

ARES Automatic Resistivity and IP System
GF Instruments, s.r.o.
Ječná 29a, 621 00 Brno, Czech Republic
www.gfinstruments.cz
(see Technical Specifications at end of this section)

LESSON PLAN:

Not all Holocene or Quaternary faults reveal themselves at the surface. Geophysics (airborne and ground) is our only tool for locating these hidden active fault traces. In this Training Session we will first compare the pattern of faulting visible at the surface to that imaged by airborne geophysics.

Once fault traces have been mapped and potential trench sites chosen, geophysics is recommended to probe the subsurface at each potential trench site. Information from geophysics about the location and depth of fault & fold structures is very helpful in planning the extent and depth of the trench, and the machinery needed to excavate the trench.

For PATA Days-2016 we will highlight the use of Electrical Resistivity Tomography (ERT) to reveal subsurface deformation. Instructors will also discuss which shallow geophysical methods will likely be most appropriate in various sedimentologic and geomorphic settings.

AIRBORNE GEOPHYSICS OF THE NORTHERN SAN LUIS VALLEY (From Grauch and Ruleman, 2013)

"The northern half of the San Luis Basin Forms an asymmetric, east-tilted half graben, with 6-7 km of total displacement. The Sangre de Cristo fault zone (Figure 1) is commonly cited as the eastern margin of this half graben, extending in length from 79 to 104 km, depending on whether it is defined by orientations of the range front, slip rates, or geomorphic expression. Sediments that filled the Miocene-Pliocene basin consist of poorly consolidated sands, silts, and gravels of the Santa Fe Group. Deposits of this age are found at high elevations to the east and north of the study area, suggesting that early rifting had a different orientation and locus of deposition in this region before Pliocene time. The study area is located where the basin narrows dramatically (Figure 1 inset) and marks the southern end of a poorly understood zone of transition from the strongly east-tilted half-graben of the central San Luis Basin on the south, to a strongly west-tilted half-graben in the next basin to the north."



INQUA Focus Group on Paleoseismology and Active Tectonics



paleoseismicity.org

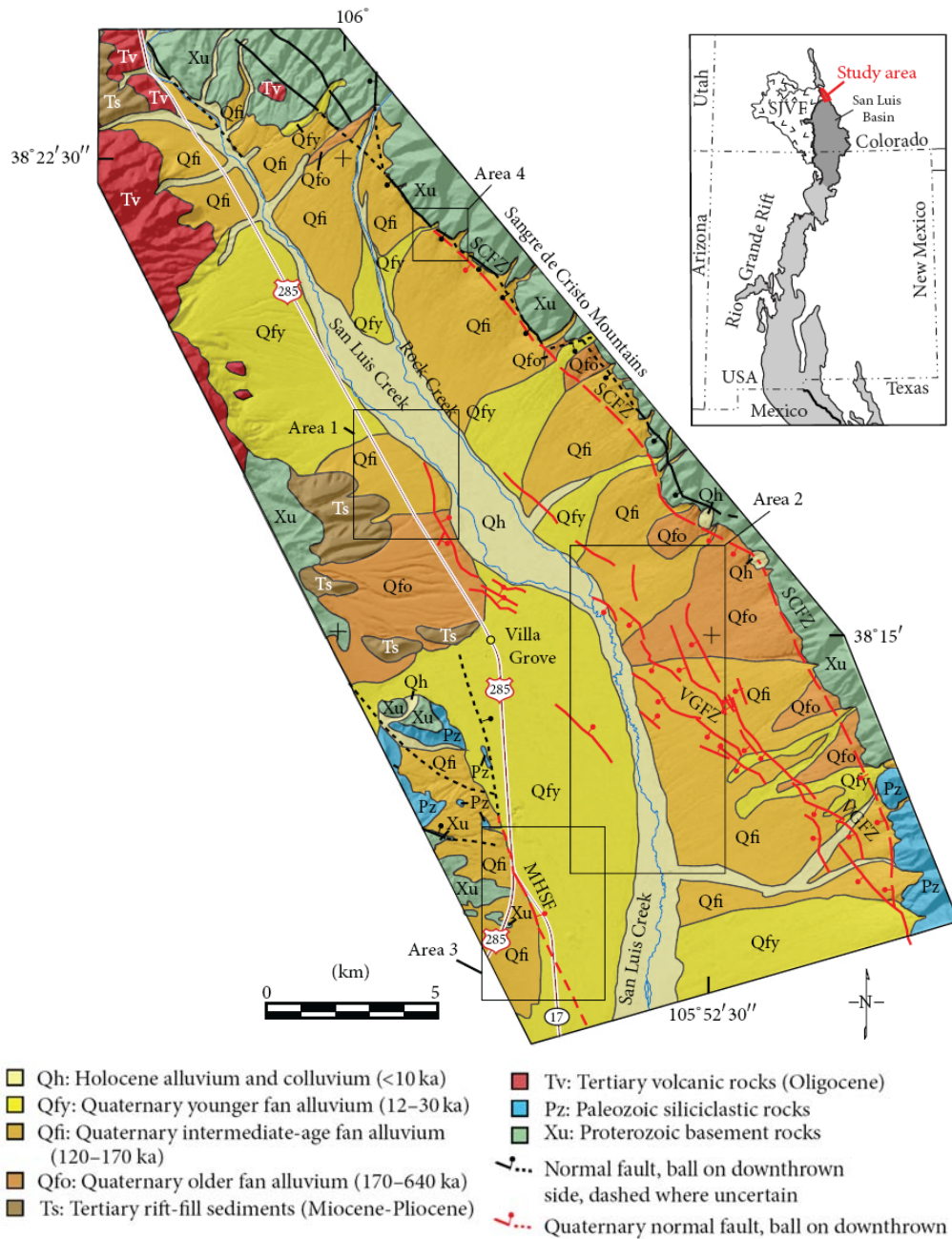


Fig. 2-1. Geology of the northern San Luis Valley area from published sources. Modifications and additions to these mapped Quaternary (active) faults and general surficial geology are presented in Grauch and Ruleman, 2013). Underlay of shaded-relief terrain is a graphically smoothed, NW-illuminated hillshade derived from LiDAR data. MHSF: Mineral Hot Springs fault, SCFZ: Sangre de Cristo fault zone, and VGFZ: Villa Grove fault zone. Boxes locate example Areas 1–4. Inset shows the location of the study area within the San Luis Basin and Rio Grande rift (basins are shaded). SJVF: San Juan volcanic field.



“Several periods of Pleistocene glaciation in the region are recorded by deposits of stream and fan alluvium, till, and outwash, which are mainly preserved near the mountain fronts. The relative ages of these deposits are determined from geomorphology and degree of weathering and soil development. From the youngest to the oldest, these deposits are Qfy, Qfi, and Qfo (Figure 1) and are associated with Pinedale, Bull Lake, and pre-Bull Lake glaciations, respectively. Based on regional correlations from previous and recent work, the glaciations in this area correspond to the following age ranges:

Pinedale (12–30 ka),

Bull Lake (about 120–170 ka),

pre- Bull Lake (170–640 ka) [21, 24–31].

The most recent (<10 ka)

deposits in the area are Holocene stream and fan alluvium deposits, unit Qh (Figure 1).”

“Precipitous, faceted spurs aligned along the range front mark the steeply west-dipping northern Sangre de Cristo fault zone on the east side of the valley (Figure 1). The northwest –trending Villa Grove fault zone, composed of multiple, mainly southwest-facing scarps developed in fan deposits, diverges from the northern Sangre de Cristo fault zone near the southeastern corner of the study area. The zone extends northwestward across the valley for about 10 km, in apparent connection with easterly facing scarps on the west side of the valley near Villa Grove (Figure 1). Kellogg suggests that much of Rio Grande rift structure is inherited from preexisting Laramide thrust fault geometry, but with reversed sense of motion.”

The Underlying Cause of Aeromagnetic Anomalies (from Grauch and Hudson, 2007)

“Faults produce linear anomalies in sedimentary basins owing either to tectonic juxtaposition of strata with differing magnetic properties or to alteration of magnetic properties along the fault plane (Gunn, 1997). Lack of exposure commonly prevents distinction between these two origins (Mushayandebvu and Davies, 2006). In contrast, serendipitous exposures in the central Rio Grande rift have provided opportunities to establish that the fault-related anomalies are principally explained by tectonic juxtaposition (Grauch et al., 2001; Hudson et al., 2008; Grauch et al., 2006).

In profile form, the linear anomalies in the central Rio Grande rift demonstrate a range in shape, from a single curving ramp to multiple ramps and peaks associated with one apparent anomaly in map view (Fig. 6). The range of anomaly shapes can be explained by differences in the relations between the thicknesses and magnetic properties of strata juxtaposed at faults (Grauch et al., 2001). These differences can even explain the presence of aeromagnetic lows over a fault zone, a counterintuitive situation that may previously have been mistaken as the expression of alteration along the fault zone.

Juxtaposition of strata can also produce multiple, vertically stacked magnetic sources at a single fault. A detailed study of the San Ysidro fault (Grauch et al., 2006), located in the northwest part of the Rio Rancho image (Fig. 2), demonstrated that several magnetic contrasts were distributed at depth along the fault plane, caused by multiple strata juxtaposed at the fault. The aeromagnetic expression differed along strike of the fault between the southern area, where the



INQUA Focus Group on Paleoseismology and Active Tectonics



paleoseismicity.org

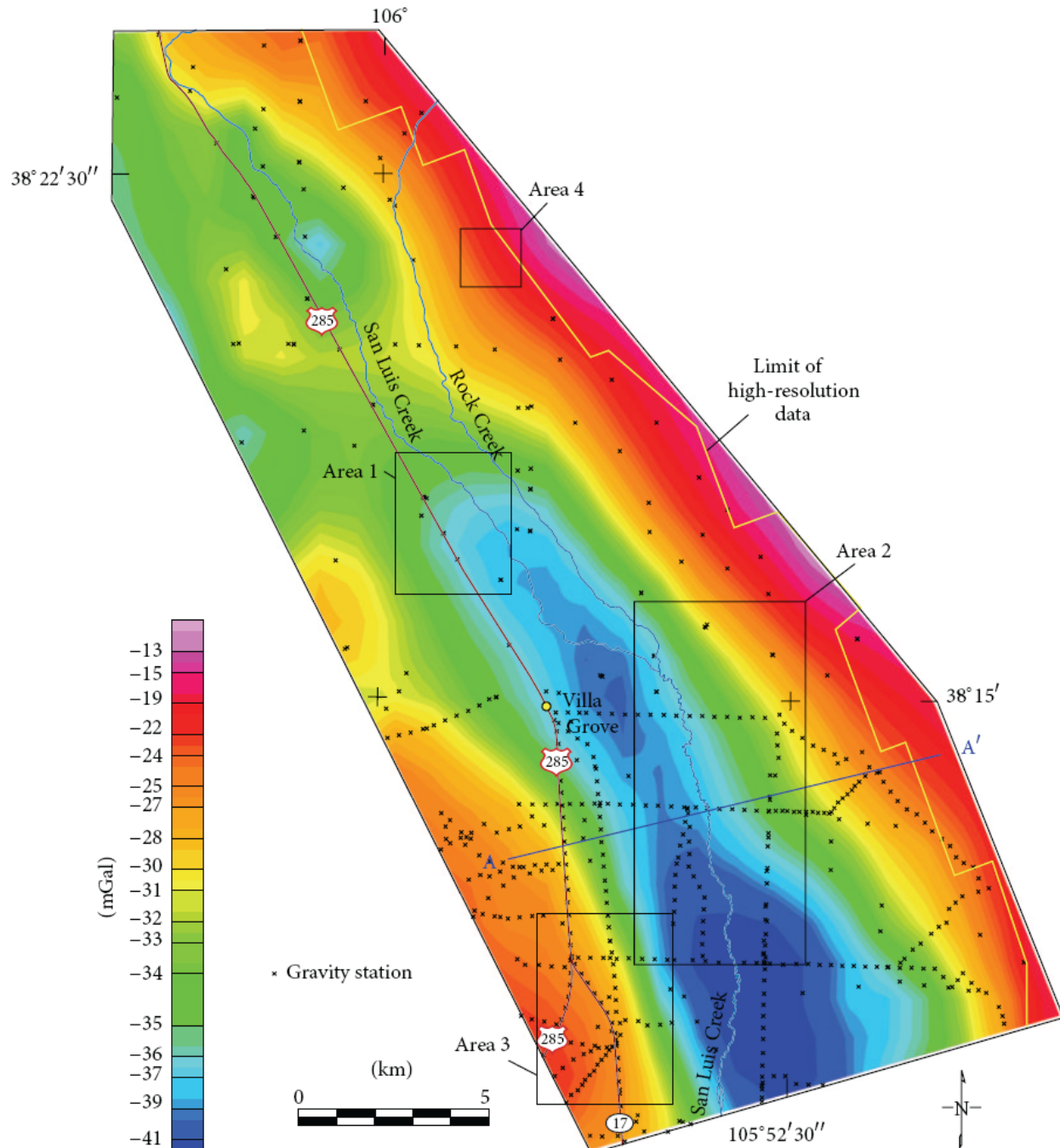


Figure 2-2: Isostatic residual gravity data showing station coverage. Boxes locate example Areas 1–4. Model for A-A' is shown in Figure 16.



INQUA Focus Group on Paleoseismology and Active Tectonics



paleoseismicity.org

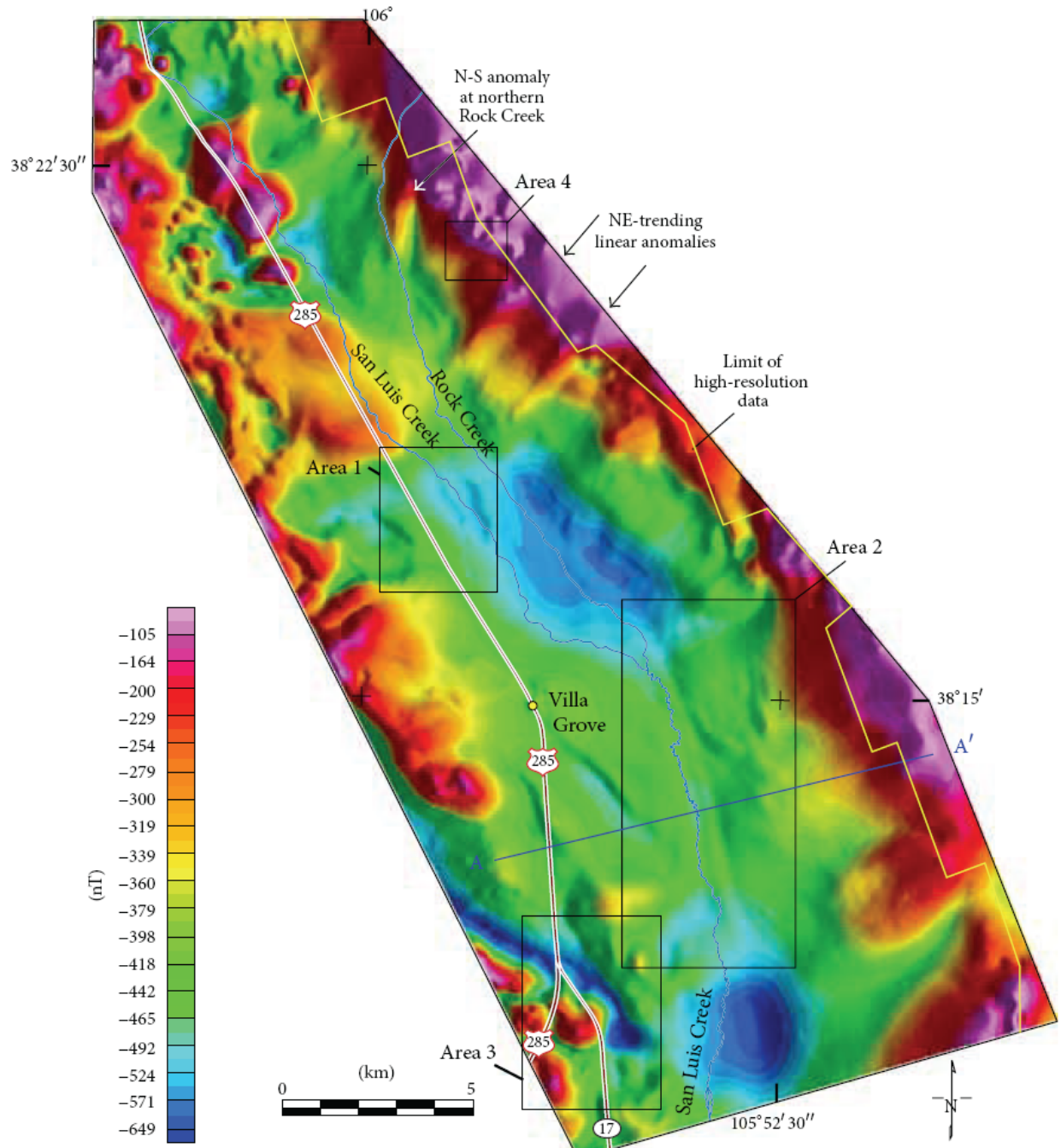


Figure 2-3: Reduced-to-pole (RTP) aeromagnetic data for the study area. Illuminated from the east. Data from the modern high-resolution aeromagnetic survey was merged with older, analog data west of the survey boundary (yellow line), described in text. Boxes locate example Areas 1–4. Model for A-A' is shown in Figure 16.



INQUA Focus Group on Paleoseismology and Active Tectonics



paleoseismicity.org

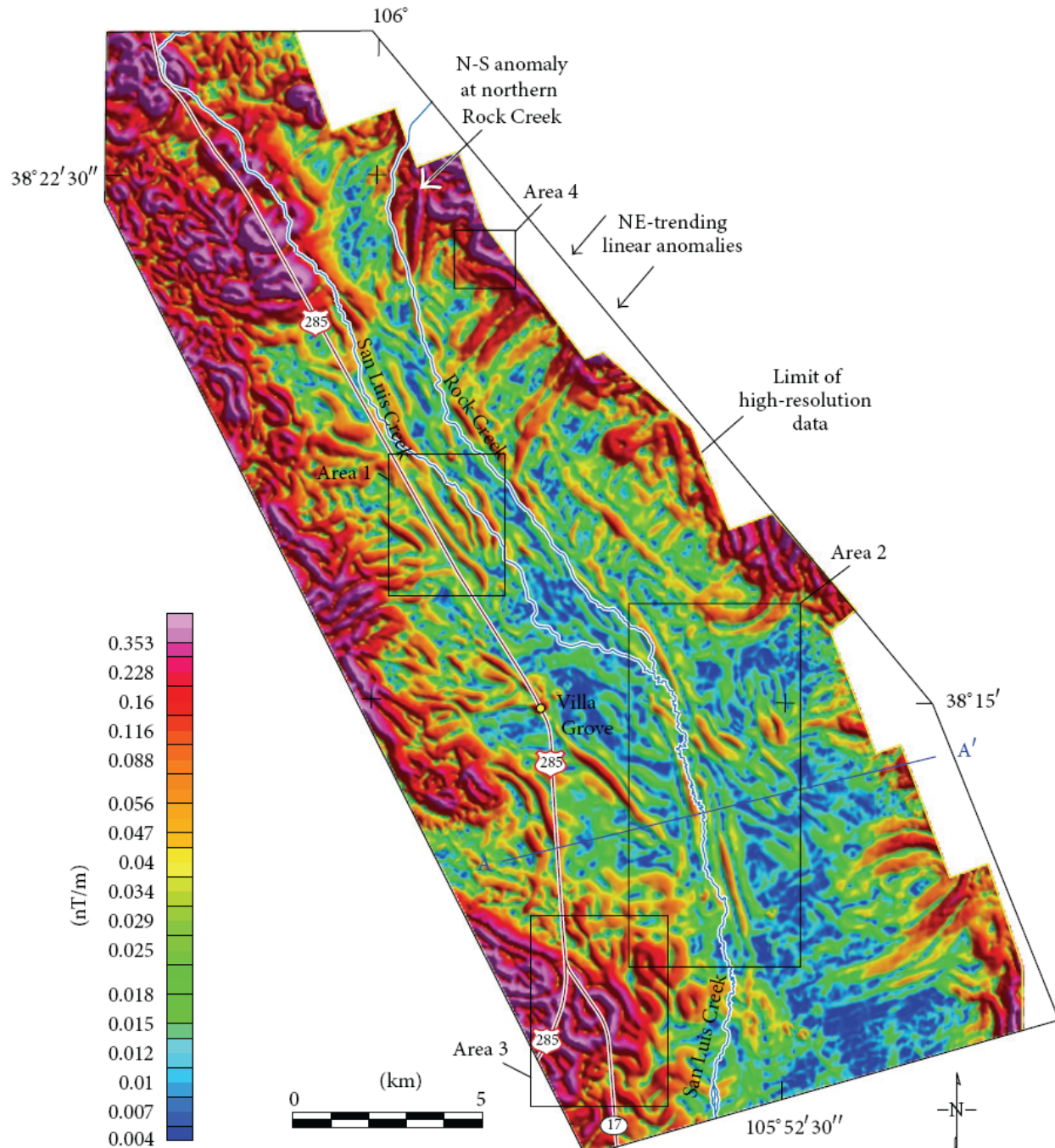


Figure 2-4: Horizontal gradient magnitude (HGM) of reduced-to-pole, high-resolution aeromagnetic data, using the gradient window method (window size = $1,225 \times 1,225\text{m}$) to focus on gradients caused by shallow sources. HGM image is illuminated from the northeast. Boxes locate example Areas 1–4. Model for A-A' is shown in Figure 16.



INQUA Focus Group on Paleoseismology and Active Tectonics



paleoseismicity.org

entire stack of juxtaposed strata was preserved, and the northern area, where erosion had removed the overlying strata, bringing the underlying juxtaposed strata closer to the surface.

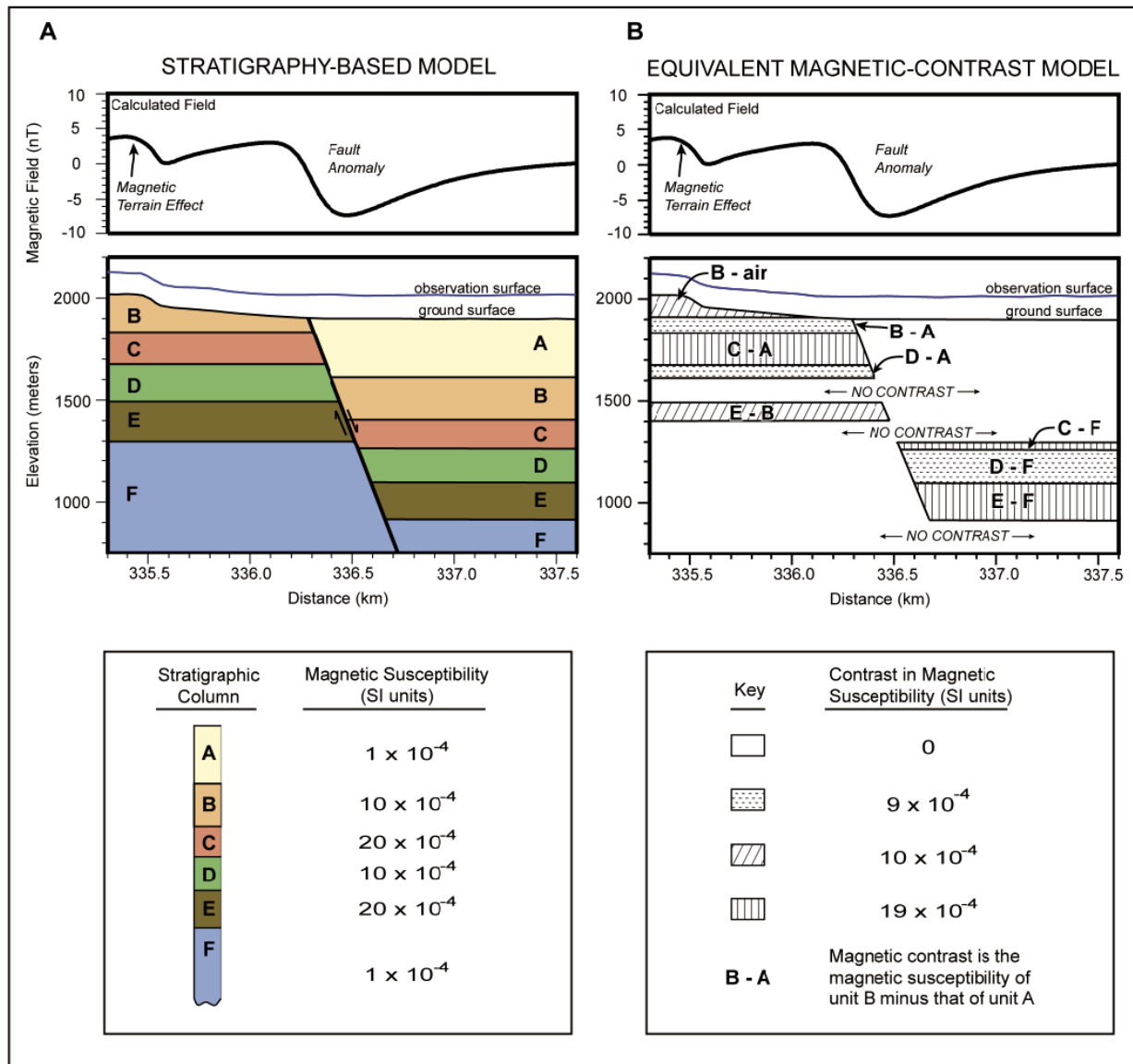


Figure 2-5. Magnetic-contrast layers derived from a geologic model. (A) Hypothetical geologic model of an intrasedimentary fault with 400 m of vertical throw. (B) Its equivalent geophysical model to demonstrate the concept of lateral magnetic contrast. The matching computed curves for both models (observed at 100 m above ground) demonstrate the equivalency of the models. Magnetic-contrast layers are constructed by inspecting only the lateral contrast in magnetic susceptibility between juxtaposed strata in (A). Where two juxtaposed strata have different susceptibilities, the magnetic-contrast layer is assigned to the side of the fault having greater susceptibility in (B). Its thickness is determined by the vertical extent of the juxtaposition between the two strata. Note the contribution of magnetic terrain effects from the hill composed of strata B, which has a magnetic susceptibility contrasting with adjacent nonmagnetic air. From Grauch and Hudson, 2007.



INQUA Focus Group on Paleoseismology and Active Tectonics



paleoseismicity.org

The primary factors driving the aeromagnetic expression of faulted strata involve differences in how the strata are juxtaposed at the fault, the magnitudes of the magnetic-property contrasts, and the depths where the contrasts occur (Grauch et al., 2001; Grauch et al., 2006). The effect of fault dip becomes increasingly important with greater depth of the magnetic contrast.

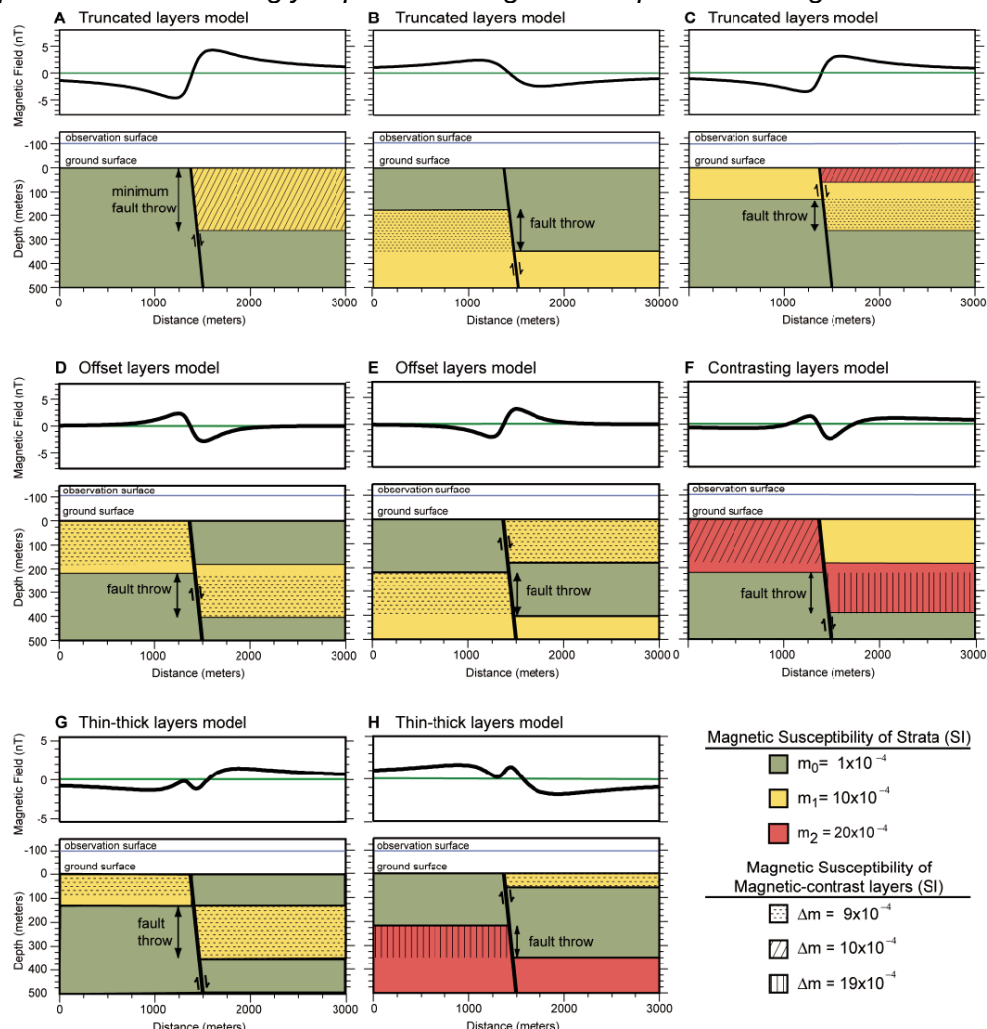


Figure 2-6. Gallery of hypothetical stratigraphy-based models (colors) that are equivalent to the four types of simple magnetic-contrast models (patterns) of Fig. 2-5. Magnetic susceptibility values (SI units) are assigned to each hypothetical stratigraphic unit and give rise to equivalent contrasts for the magnetic-contrast layers. Fault throw is indicated for each geologic model. Truncated-layer geophysical models arise from hypothetical geologic models of (A) an eroded normal fault, (B) an eroded normal fault or a growth fault, (C) an eroded normal fault or a growth fault with magnetic colluvium on the hanging wall. Offset-layers geophysical models arise from hypothetical geologic models of (D) a normal fault with alternating weakly and moderately magnetic units, and (E) a normal fault with the opposite alternation of strata. A contrasting-layers geophysical model arises from a hypothetical geologic model of (F) a normal fault offsetting a magnetic unit, with moderately magnetic colluvium on the hanging wall. Thin-thick layers geophysical models arise from hypothetical geologic models of (G) an eroded normal fault, and (H) an eroded normal fault or a growth fault with moderately magnetic colluvium on the hanging wall. From Grauch and Hudson, 2007.



In the central Rio Grande rift and perhaps in sedimentary basins in general, this effect is less important than the other factors because faults are commonly steeply dipping and magnetic contrasts are generally shallow, as discussed below. In the following sections, we examine these factors in terms of the main geophysical parameters that drive anomaly variability, and then discuss the geologic and magnetic-property criteria for expression of faults in aeromagnetic data.”

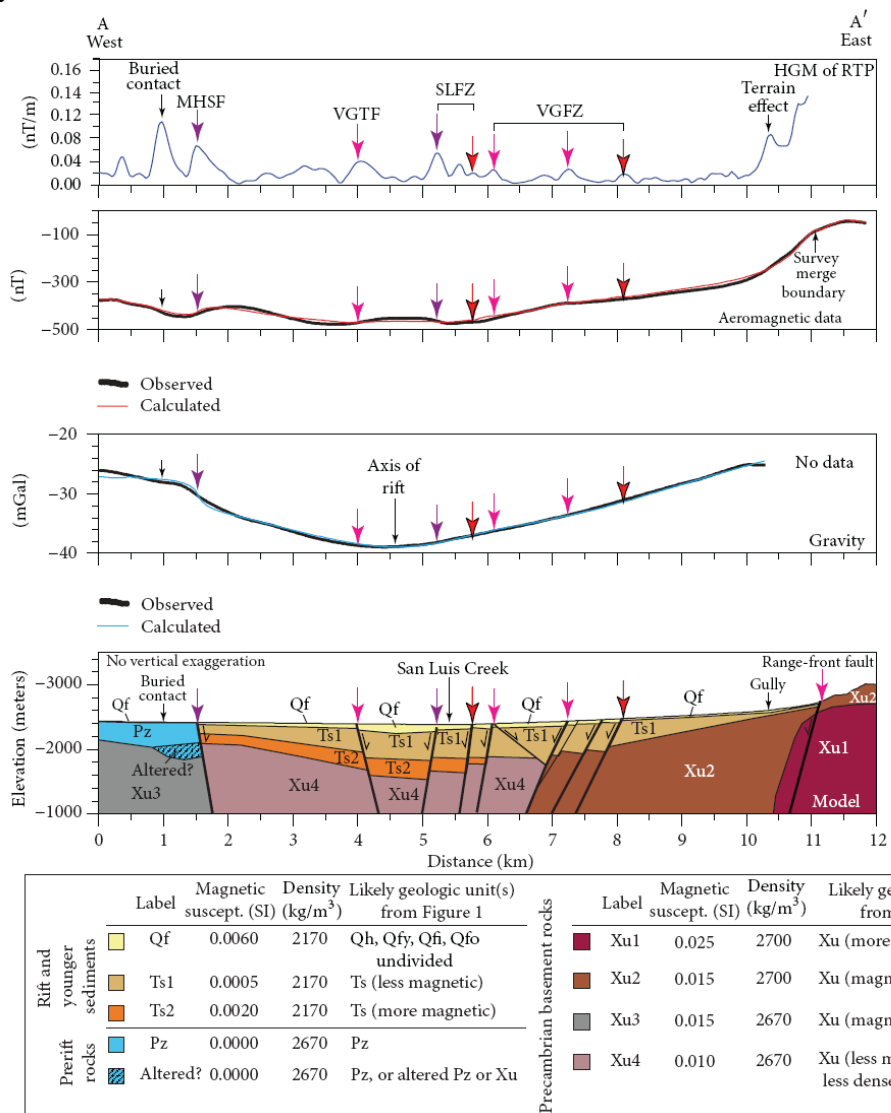


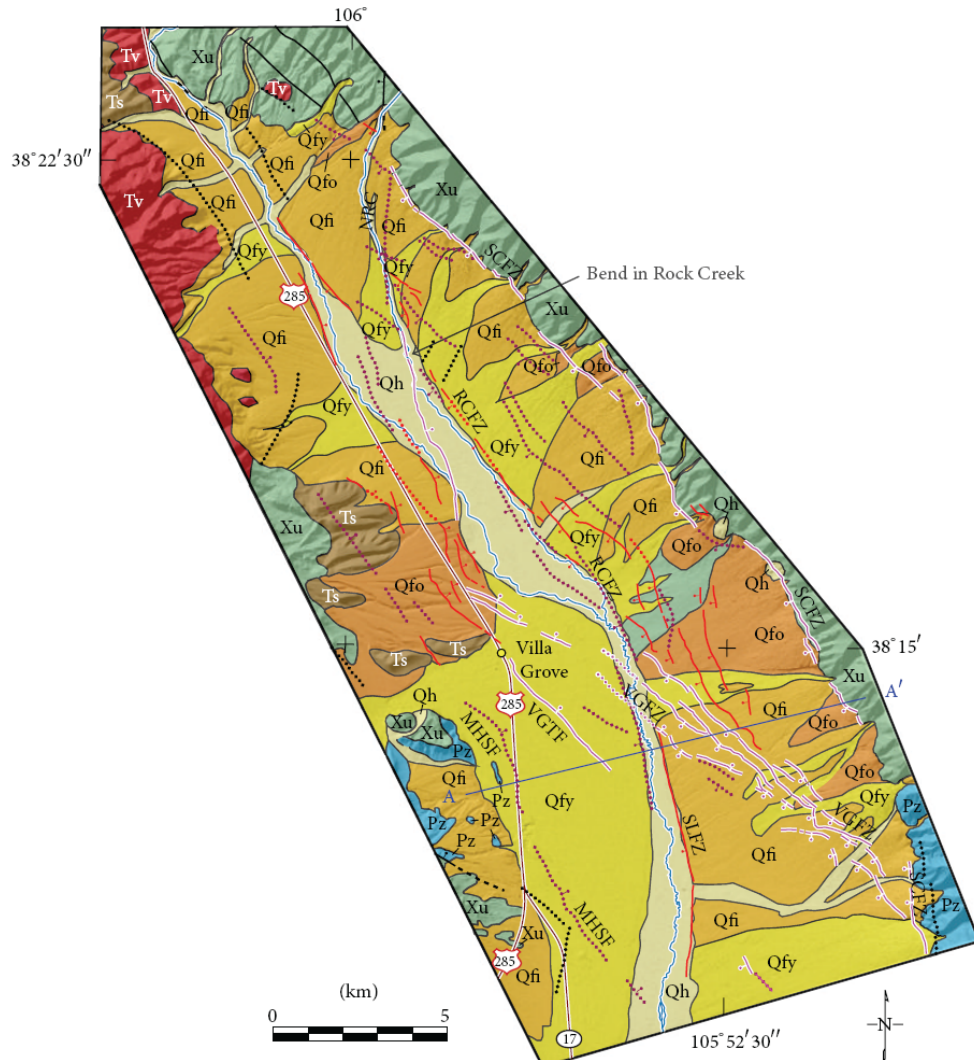
Figure 2-7. 2D geophysical model for profile A-A' (located in Figures 2–4, 6, and 15). Observed curves were extracted from the grids for reduced-to-pole aeromagnetic data (Figure 2), isostatic residual gravity (Figure 4), and HGM of the reduced-to-pole aeromagnetic data (HGM of RTP) (Figure 6). MHSF: Mineral Hot Springs fault (revised), SLFZ: San Luis Creek fault zone, VGFZ: Villa Grove fault zone, and VGTF: Villa Grove town fault. Colored arrows point to the locations of inferred faults from Figure 15, coded in a similar fashion: magenta indicates active (younger), red (with black outline) active (older), and purple potentially active.



INQUA Focus Group on Paleoseismology and Active Tectonics



paleoseismicity.org



Age of most recent activity

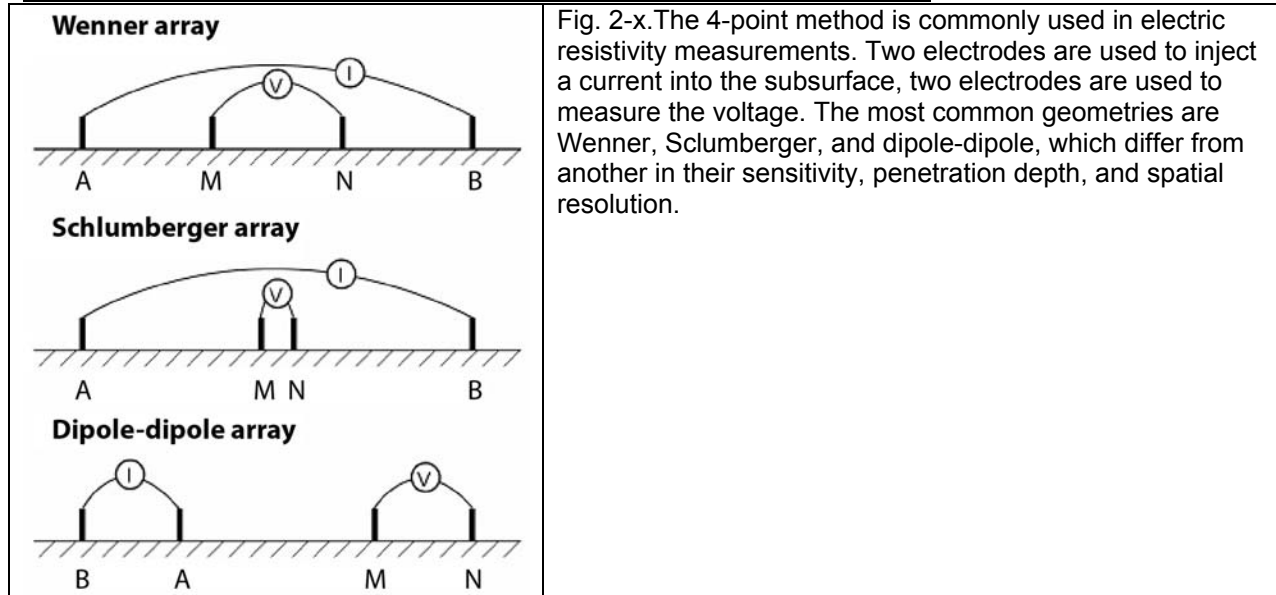
- Active (younger): scarps well developed and displace units Qfy (<30 ka) or Qh (<10 ka). Concealed segments inferred from aeromagnetic data
- Active (older): scarps degraded and/or displace only units older than Qfy (>12 ka) or Qfi (>120 ka). Concealed segments inferred from aeromagnetic data
- Potentially active: no scarps evident, but fault and relation to active faults are inferred from aeromagnetic data. Sense of throw inferred from gravity data.
- Inactive: fault geologically mapped or inferred from aeromagnetic data in prerift rocks

Normal fault: ball on downthrown side, dashed where uncertain, dotted where concealed

Fig. 2-8. Revised surficial geology and inferred active faults and buried fault segments resulting from combined interpretation of the aeromagnetic and LiDAR data for the study area. MHSF: Mineral Hot Springs fault (revised), NRC: Northern Rock Creek; RCFZ: Rock Creek fault zone, SCFZ: Sangre de Cristo fault zone, SLFZ: San Luis Creek fault zone, VGFZ: Villa Grove fault zone, and VGTF: Villa Grove town fault. Model for A-A' is shown in Figure 16.



GROUND-BASED GEOPHYSICS FOR SITE-SCALE EXPLORATION



EXAMPLES of ERT APPLICATIONS IN NEOTECTONICS

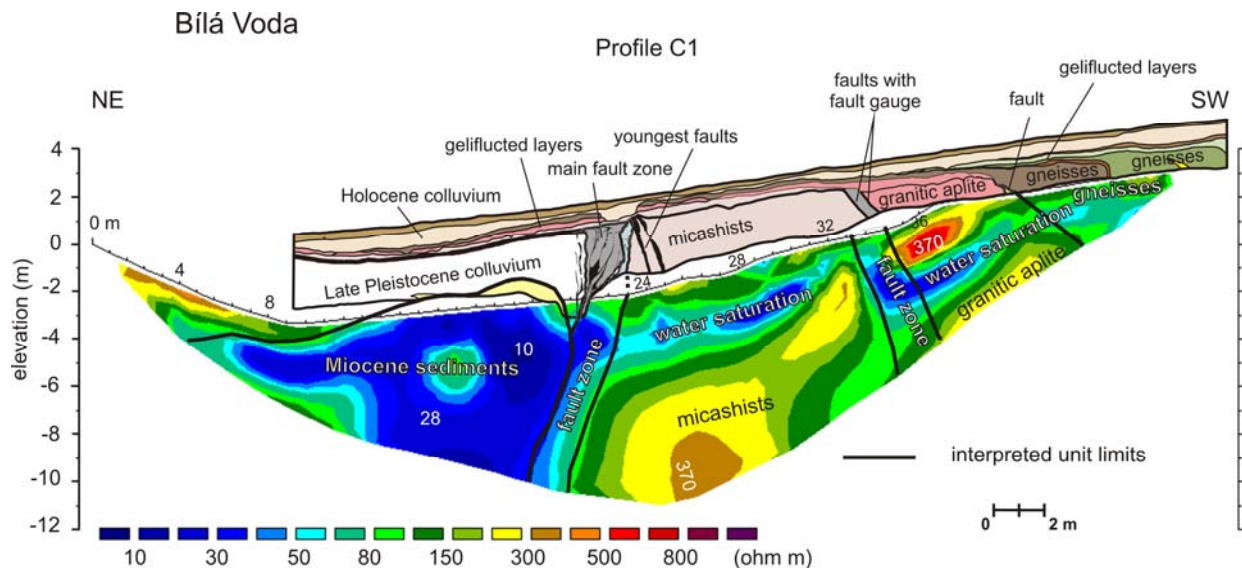


Fig. 2-x. Model resistivity of ERT at the locality Bila Voda (Bohemian Massif, Czech Republic) carried out at the floor of the paleoseismic Trench C with Wenner-Schlumberger electrode array and electrode spacing 0.8 m. Vertical exaggeration=1; iteration 5; RMS error=3.9%. Interpretation of the ERT profile to the depth is based on the logged geology exposed in the trench. From Stepancikova et al., 2011.



Projecting of water well



Detailed geological information for locating, drilling and building of water well was required. The preliminary idea of the survey was based on mapping of tectonic zones and weathered rocks. Due to the needed rather high depth range and resolution Pole-Dipole method was chosen (infinite electrode C2 at $x = 50$ m and $y = 600$ m).

The picture shows the position of a wide fault filled with permeable weathered rocks convenient for building of the well with rich water supply.

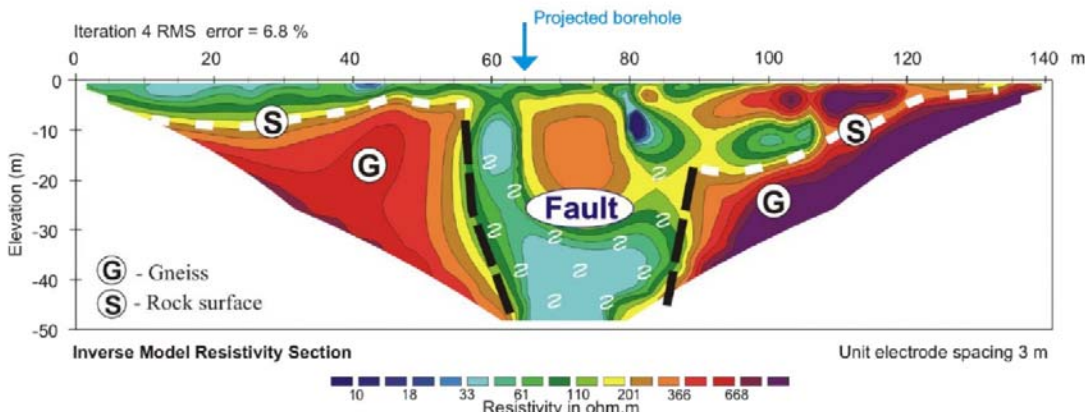


Fig. 2-8. EXAMPLES of ERT APPLICATIONS (provided by GF Instruments).

RESULTS OF PREVIOUS ERT Survey ~ 3 m SOUTH of the VGFZ Trench

In 2013 Andre Revil (then of Colorado School of Mines) performed an ERT survey parallel to the axis of the VGFZ fault trench, but offset about 3 m to the south. This was a 66 m-long array with electrode spacing of 1 m.



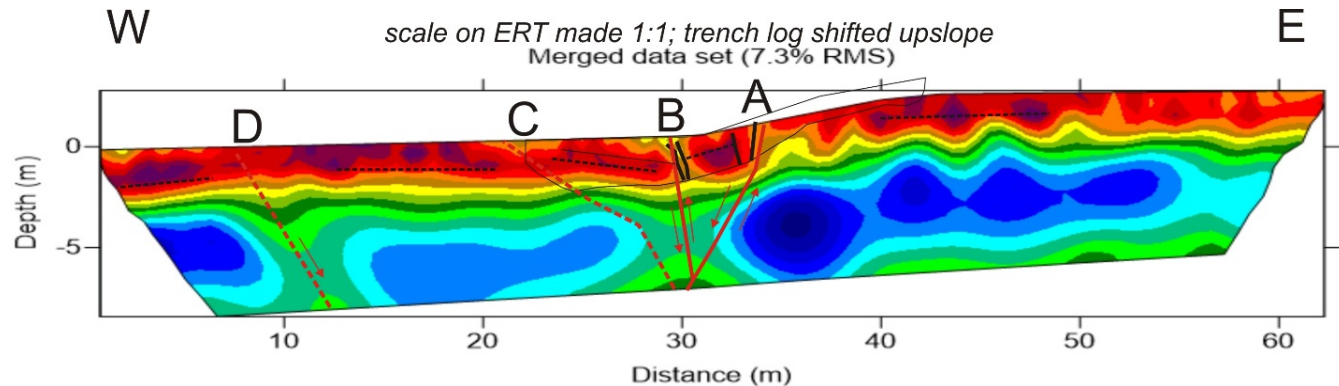
Fig. 2-9. Trench log of the VGFZ trench, mirrored to match the orientation of the ERT survey (below).



INQUA Focus Group on Paleoseismology and Active Tectonics



paleoseismicity.org



INTERPRETATION: 1- on Fault A, refraction that created the graben occurred just below the trench floor; Fault A must flatten downward to avoid penetrating the low-resistivity deposits of the footwall (dark blue); 2- Fault B probably steepens with depth, to stay in the center of the medium-resistivity zone (green); 3- bedding (dashed black lines) on the footwall and hanging wall is essentially horizontal, but in the fault zone is shown to dip. Between Faults A and B the apparent dip is 14 degrees toward the hanging wall, and between Faults B and C is 7 degrees toward the footwall. Both of these tilts are seen in the trench wall, but not as extreme. In other words, the ERT appears to exaggerate the dips. 4- the ERT implies two additional structures (dashed red lines) not exposed by the trench. Fault C is inferred because the dips toward the footwall (between B and C) do not continue farther west, but flatten out. Also, the medium-resistivity zone beneath Fault B seems too wide to just be caused by Faults B and C. This inferred "fault" may be a simple extensional hinge zone, and was not recognized in the far western end of the trench. Fault D is inferred from the existence of another medium-resistivity zone 15 m west of Fault C, and the fact that bedding appears to steepen again west of this zone. Also, west of Fault D the low resistivity strata (dark blue) again reach the same values as seen on the footwall, whereas east of fault D the same beds are less resistive, suggesting they have been affected by faulting. The ERT suggests that the fault zone here actually spans from 10 m to 32 m on the horizontal scale (22 m wide), as opposed to the fault scarp which is only 10 m wide.

Fig. 2-10. ERT survey alongside the trench axis.



ARES Traditional single channel resistivity & IP system equipped with a variety of smart and economic accessories. One ruggedized weatherproof unit integrates transmitter with receiver and control unit completed with rich software support for many measuring methods.

ARES - Technical Specifications

Transmitter

Power up to 850 W

Current up to 5 A (24 bit resolution)

Voltage 2000 Vp-p (actually applied voltage automatically optimizes level of measured potential)
full electronic protection, energy efficiency up to 91%, passive cooling without ventilation holes

Receiver

Input voltage range □5 Vp-p (24 bit resolution), □10 Vp-p optionally

Input impedance 20 M Ω

Mains frequency filtering 50 or 60 Hz selectable notch filter

Measuring methods 2D/3D Multi-Electrode Resistivity and IP Tomography

VES – Vertical Electrical Sounding (resistivity and IP)

RP – Resistivity and IP Profiling

SP – Self Potential

cross-hole tomography

Supported arrays Wenner Alpha / Beta / Gamma, Wenner-Schlumberger, Dipole-Dipole, Pole-Dipole, Reverse Pole-Dipole, Pole-Pole, MGM, Equatorial Dipole-Dipole, Cross-Hole, Borehole-Surface, user defined configurations

Measurement - features checking of grounding

automatic calibration

automatic pulse cycling and checking of measured values

easy interruption and continuation of measurement

capability of profile prolongation by means of multi-electrode cable rolling

Total accuracy better than 1% (typically)

IP - Induced Polarization (Chargeability) up to 10 adjustable IP-windows, each max. 30 s, step 20 / 16.66 ms

Pulse 0.3 s – 30 s, step 0.1 s

SP compensation constant and linearly varying SP cancellation

Stacking manual or automatic (with self-adaptive setting)

adjustable optimum measured voltage and maximum acceptable measurement error

Stored values position of the measured point, output current, input voltage, SP, apparent resistivity, standard deviation, chargeability with standard deviation for up to 10 IP windows

Number of electrodes max. 200 in one array

Control unit easy-control system

alphanumeric keyboard, large LCD display

measuring system can be upgraded via internet

safety switch

Memory 16 Mbit, up to 100 files, 70000 readings

PC Interface RS232 and USB

PC software provides data download and export for processing programs (RES2DINV / RES3DINV, Surfer, IPI2WIN and others) as well as upload of measuring procedures

Power supply 12 V car battery or 12 V attachable battery pack, 12 V electronic power supply, AC/DC adapter for office

Connectors for PC, battery and a universal one for all measuring accessories (Multi-Electrode Cable, VES-Adapter, Switch box), current and potential sockets

Dimensions 15 x 21 x 40 cm

Weight 5.9 kg

Ambient conditions -10°C to +50°C, weatherproof



INQUA Focus Group on Paleoseismology and Active Tectonics



paleoseismicity.org

3-PALEOSEISMIC TRENCH LOGGING TECHNIQUES; MANUAL VS 2D PHOTOMOSAIC VS 3D STRUCTURE FROM MOTION

INSTRUCTORS:

Dr. James McCalpin (GEO-HAZ Consulting)
Brian Gray (Lettis Consultants International)

EQUIPMENT:

Tape measure
Graph paper
Pencil
Digital camera

LESSON PLAN:

Dr. James McCalpin (GEO-HAZ Consulting) will discuss the scientific strategy for siting paleoseismic trenches, i.e. is trench meant to capture displacement (spatial) or recurrence (temporal) data? The investigator can customize the trench design to obtain the desired data, but trench design is also limited by material cohesion, depth to groundwater, and government safety regulations.



Fig. 3-1. When all else fails, you can make a trench log with manual mapping on graph paper. This 2D technique is the least orthographic and georeferenced of all techniques, but is still the best for showing the critical geologic contacts that define the sequence of events, which is the whole point of trenching. Planimetric precision and accuracy are less important, because if the trench were located several meters in either direction along strike, those values would likely be different. But the number of displacement events and their ages would remain the same, and that is the paleoseismic "story."



Even with manual logging, it is advisable to supplement the log by drawing on photos taken on your ipad. In any case, take countless photos of all the trench walls at all scales during all stages of the investigation for later office study.

We will perform several types of trench logging in the teaching trench on the Villa Grove Fault Zone (Fig. 3). This trench, excavated in 2001, is the only permanent paleoseismic trench in North America, and has been used for the past 15 years to train paleoseismologists. In 2013 an electrical resistivity tomography (ERT) survey was run adjacent to the trench, the results of which are enlightening (previous section).

INTERPRETIVE PRINCIPLES

The three steps critical for interpreting trench-wall relationships are:

- (1) Identify Unconformities Created by Each Earthquake (“Event Horizons”)
- (2) Date Event Horizons by Bracketing Samples (Above and Below Horizon)
- (3) Measure Displacement in Each Event by Retrodeforming the Trench Log

(1) Identify Unconformities Created by Each Earthquake (Event Horizons)

(2) Date Event Horizons by Bracketing Samples (Above and Below Horizon)

(3) Measure Displacement in Each Event by Retrodeforming the Trench Log

Because soil horizons change thickness across the fault, multiple small fault movements probably occurred during the deposition of this stratigraphic sequence. In theory the timing and amount of these small displacements could be reconstructed using a wireframe technique (McCalpin and Harrison, 2001). A wireframe rendition of the trench log contains only the unconformities, making it slightly easier to see displacement patterns than working with the entire trench log. For measuring displacements, this technique is faster than a full trench log retrodeformation analysis. Zia fault, Albuquerque New Mexico.

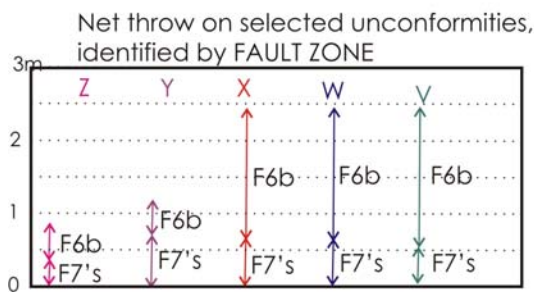
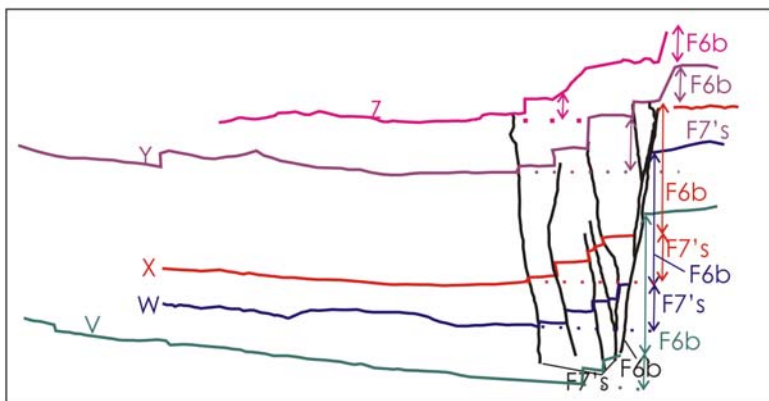


INQUA Focus Group on Paleoseismology and Active Tectonics

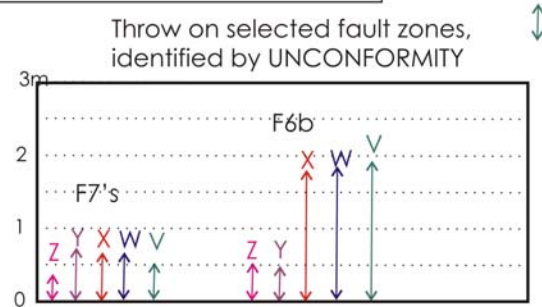


paleoseismicity.org

Wireframe diagram of unconformities and faults (zone F7's and fault F6b only)



Interpretation: 1) net throw on horizons X, W, and V is identical, therefore the first movement on these faults was in EVENT X



Interpretation, Fault zone F7's: 1) throw on horizons Y, X, W and V is identical, therefore the first movement on this fault was in EVENT Y.
2) throw in EVENT Z was 0.6 m; in EVENT Y, 0.6 m; Cumulative throw, 1.2 m.

Interpretation, Fault F6b: 1) throw on horizons X, W and V is identical, therefore the first movement on this fault was in EVENT X
2) throw in EVENT X was 2.6 m; in EVENT Y, no throw; in EVENT Z, 1 m throw

Brian Gray (Lettis Consultants International) will discuss trench photography and image-processing strategies for developing high-resolution 3D photomosaic images using Structure from Motion software.



INQUA Focus Group on Paleoseismology and Active Tectonics



paleoseismicity.org

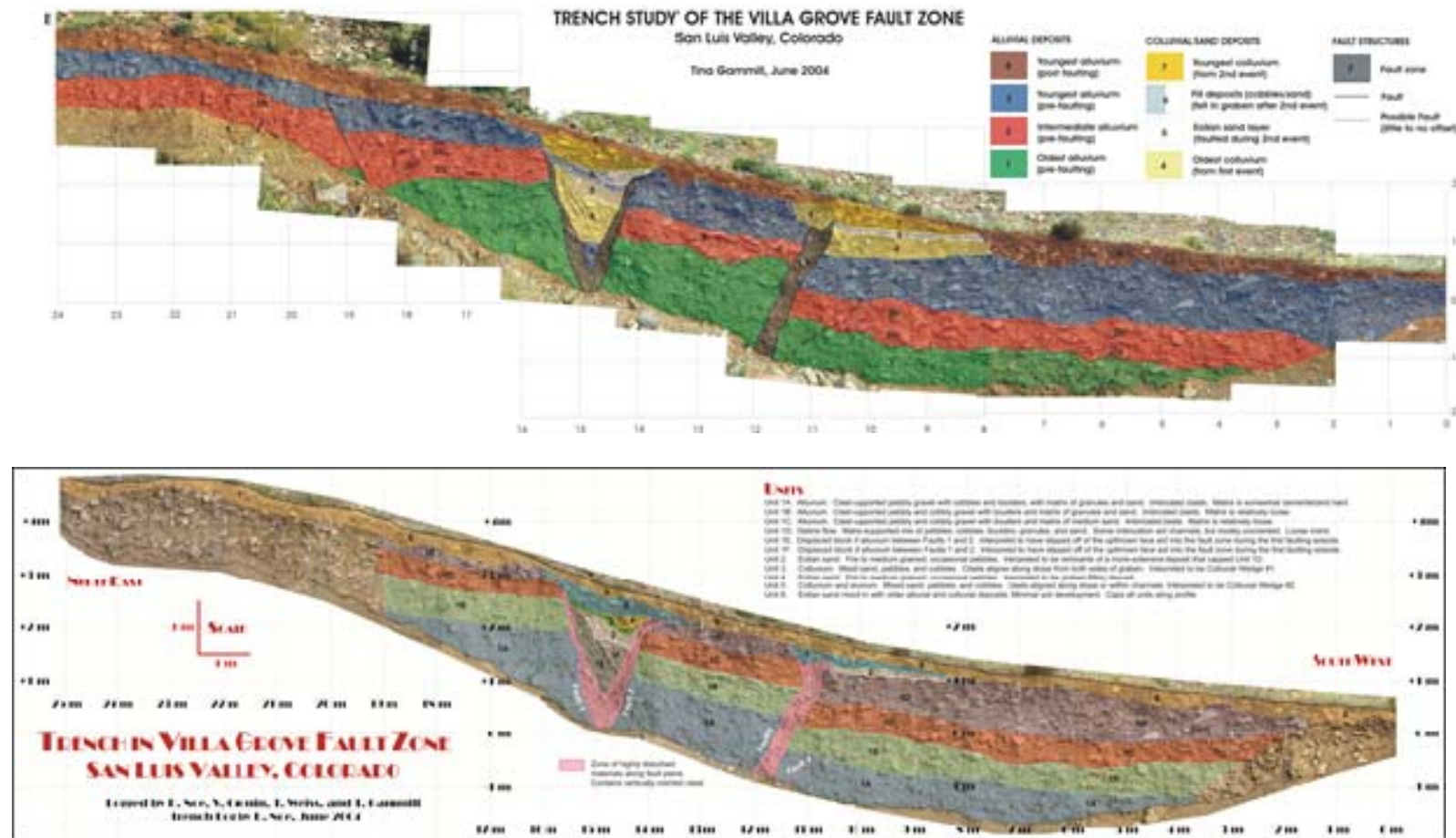


Fig. x. Examples of trench logs made by drawing geologic unit polygons atop a 2D photomosaic.



INQUA Focus Group on Paleoseismology and Active Tectonics

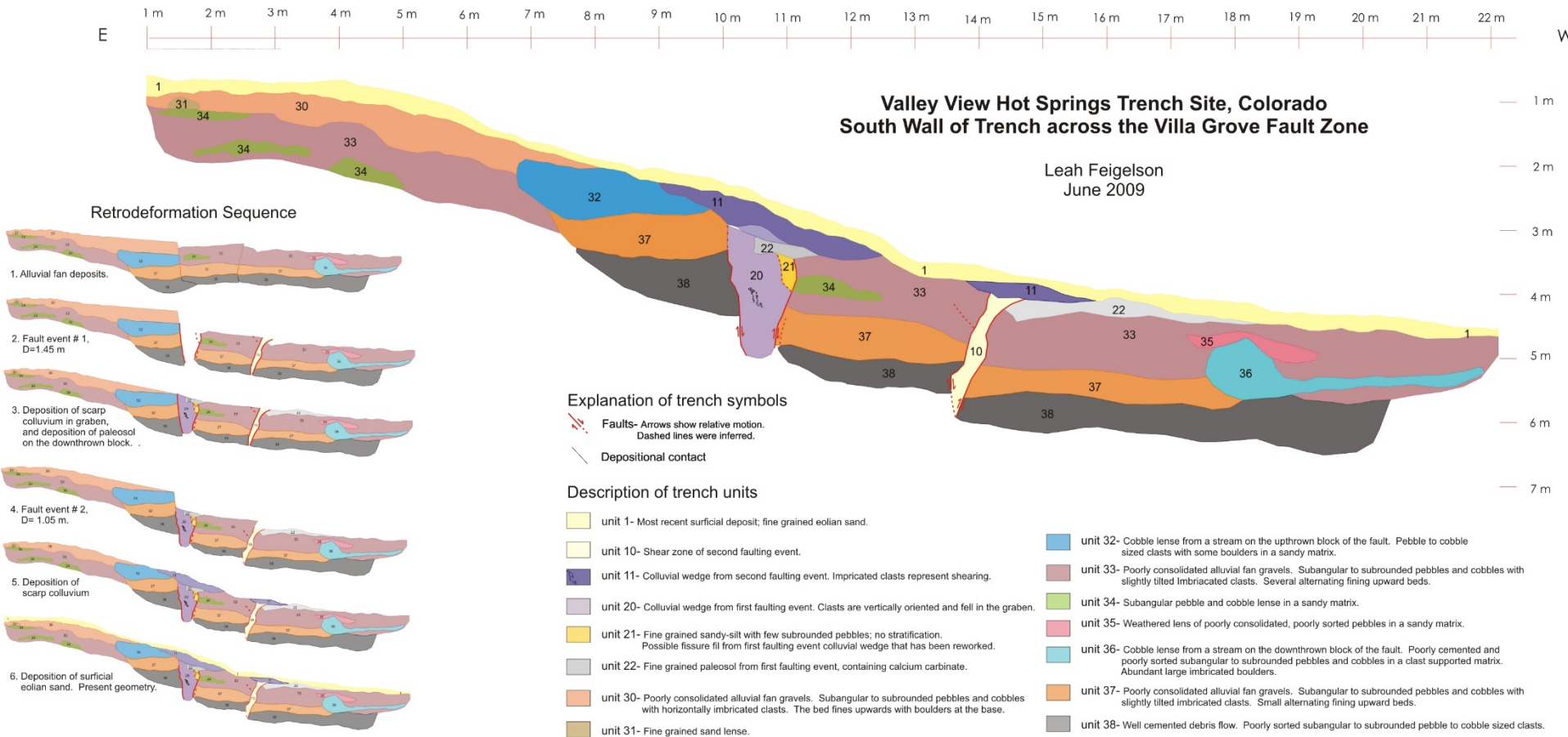
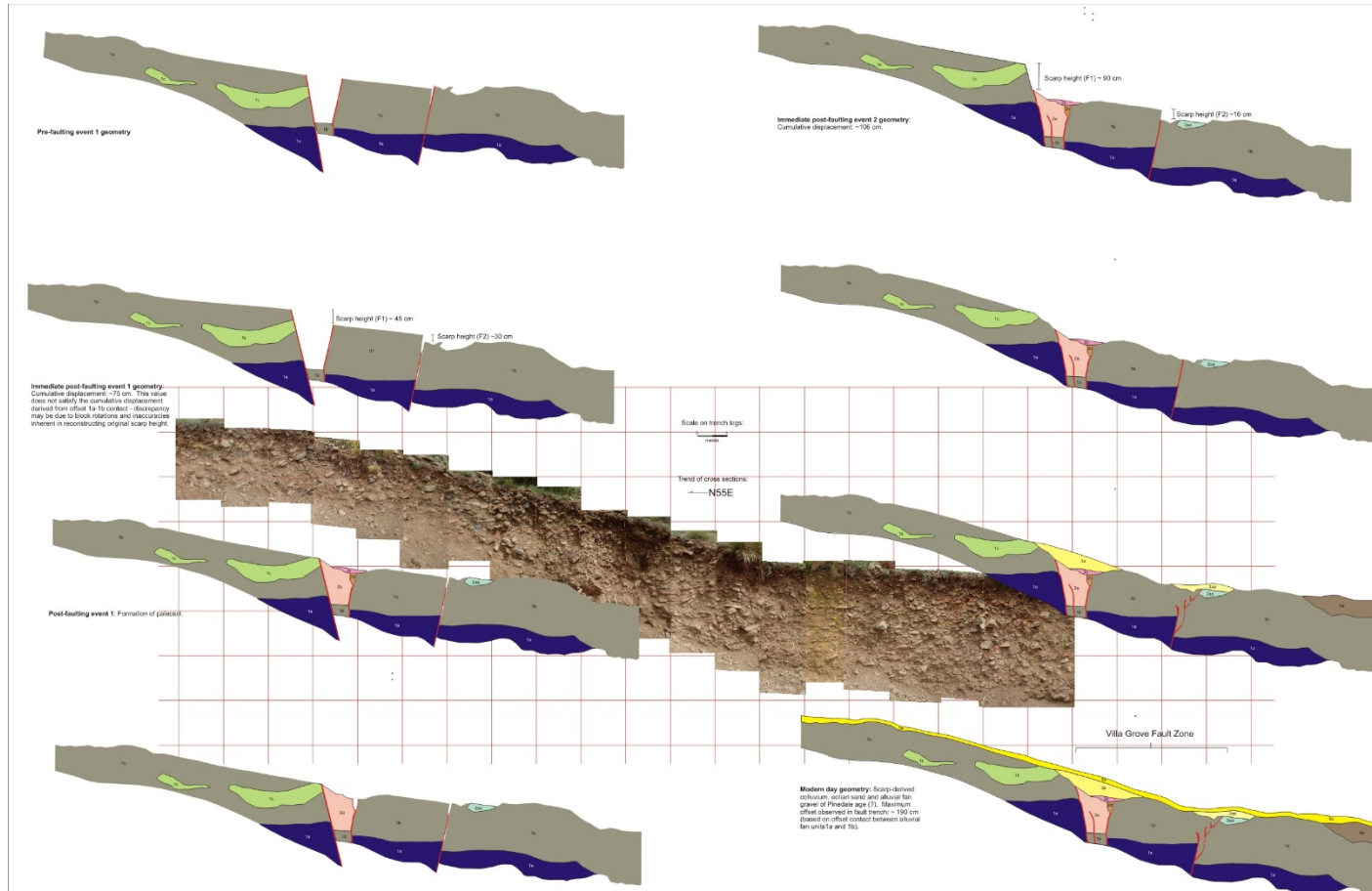


Fig. x. Example 1 of a 2D vector trench log and retrodeformation sequence.



INQUA Focus Group on Paleoseismology and Active Tectonics



Retrodeformation Analysis Villa Grove Fault Zone, San Luis Valley, Colorado

Joshua T. Goodman
June 2009

Description of trench units and symbols	
Modern surface deposits	Fault: solid where observed continuously; dashed where observed discontinuously, and dotted where inferred.
4a	transverse drainage channel
3a	modern slopewash/crevices
3a	colluvial wedge: predominantly sandy w/ isolated cobbles.
2a	channel facies/lag deposits: cobble- to boulder-sized, clast-supported (open framework); poorly sorted; unconsolidated.
2a	debris-overleated fan facies: sand- to cobble-sized, poorly sorted; matrix-supported; imbricated; poorly sorted.
2a	colluvial wedge: sand- to cobble-sized; vertically-oriented flints.
2a	colluvial wedge: predominantly sandy w/ isolated cobbles.
1a	paleosol: carbonate rinds on clasts.
1a	feature RIE (1): predominantly sandy w/ isolated gravel-size clasts; unconsolidated.
1a	channel facies/lag deposits: cobble- to boulder-sized, clast-supported (open framework); poorly sorted; unconsolidated.
1a	debris-overleated fan facies: sand- to cobble-sized, poorly sorted; matrix-supported; imbricated; poorly sorted.
1a	colluvial wedge: predominantly sandy w/ isolated cobbles.

Fig. x. Example 2 of a 2D vector trench log and retrodeformation sequence.



4-THE IMPORTANCE OF SOIL STRATIGRAPHY AND DATING IN PALEOSEISMOLOGY

4-Soil Stratigraphy and its Use in Paleoseismology

Dr. Alan Nelson (USGS-Golden) and **Dr. James McCalpin** (GEO-HAZ Consulting) will explain why soil profile development is so important in estimating ages of the geomorphic surfaces displaced by fault traces, and the ages of stratigraphic units exposed in trench walls. We will visit several soil profile exposures of different ages on alluvial fans, and discuss how soil stratigraphy can often constrain the time spans between erosional, deposition, and displacement events exposed in trench walls (Fig. 4).

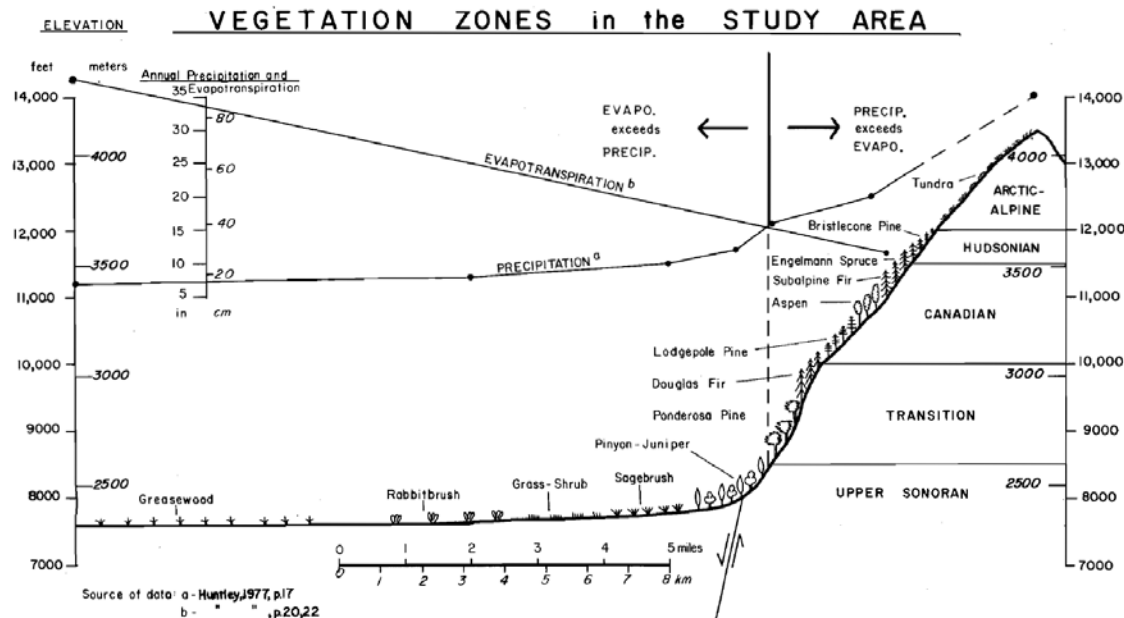


Fig. 4-1. Vegetation zones near the Sangre de Cristo fault; from McCalpin, 1981.

Table 6.—Alluvial deposits: weathering and morphologic characteristics

Age of Deposit ^a	Morphology	Slope	Eolian Cover	Soil Development	Clast Weathering	Dissection	Surface Morphology	Direct Connection to Moraines
Northern Segment								
Ha	linear flood plain	low	none	azonal	no oxidation	none	active bar-and-swale	No
Pfu	narrow channels	low	variable	weak	slight oxidation	slight	fresh bar-and-swale	No
Pf2	large symmetrical fans	2-5°	thin, discontinuous	very weak	no oxidation	very slight	fresh bar-and-swale	No
Pfl	large symmetrical fans	3-6°	33-75 cm	weak	slight oxidation	slight	smooth alluvial surface	Yes
Bf	broad bajada, interfan ridges	5-6°	variable	moderate	moderate pitting, oxidation	moderate	relict surface with paleo-channels	No
pBf	interfan wedges, fault-bounded fan remnants	7-8°	variable	very strong	severe pitting, severe oxidation		eroded ridges of alluvium	b



Developing a Soil Chronosequence to Date Offset & Non-Offset Geomorphic Surfaces

A soil chronosequence consists of a series of typical soil profiles on geomorphic surfaces of clearly different (and hopefully, known) ages. The sequence will be a true chronosequence, showing the effects of increased time of soil formation, ONLY if the other four soil-forming factors are held constant in the sequence (parent material; climate; topography; organisms). For example, in the San Luis Valley, soil profiles on alluvial fans of various ages (Pinedale, Bull Lake, pre-Bull lake) all share the same parent material, topography, and organisms. However, soils at higher elevations (fan-heads, and in the northernmost part of the valley) lie above the precipitation=potential evapotranspiration line, and thus have no calcium carbonate in the soil profile. For those soils, the key soil parameter that increases with time is pedogenic clay, most of which accumulates in textural B horizons. Soils that formed below the precipitation=potential evapotranspiration line contain accumulations of pedogenic calcium carbonate, the amount and morphology of which increase with soil age. Because of this variability in climate as well as time, we constructed two soil chronosequences for alluvial fan soils in the San Luis Valley; one for non-calcareous soils, and one for calcareous soils (Fig. 4-2).

Similarly, glacial moraines lie at higher elevations than their contemporaneous outwash on the alluvial fans, so at the moraines climate is cooler and wetter, and organisms are forest rather than grasslands. We can compare soil profiles on alluvial fans and moraines of the same age where time, parent material, and topography are constant, but climate and organisms vary. This sequence of soil profiles is called a climosequence, because the main variable is climate.

Table 9.—Summary of soil profile data on alluvial deposits^a

No. of Profiles	Age of Deposit ^b	B Horizon Thickness	B Horizon Structure ^c	Maximum Soil Color ^d	Calcareous Horizon Thickness	Horizon Stage ^e
3	Hf	None	None	10YR 5/3-10YR 5/8	46"	I
11	Pf	None to 14"	None to Bs (cambic B)	10YR 5/3-7.5YR 5/4	23"-74"	I-II
9	Bf	5"-43"	wk to str, sbk	10YR 5/4-7.5YR 5/6	50"-75"	II-III
5	pBf	47"-71"	str abk to str columnar	5YR 4/4-5YR 5/6	77"-149"	III-III+

Total = 28

^a Values listed are ranges for all soil profiles of the stated age.

^b Hf—Holocene, Pf—Pinedale, Bf—Bull Lake, pBf—pre-Bull Lake.

^c Abbreviations defined in Appendix A.

^d Munsell color.

^e Carbonate stages after Gile and others 1966.

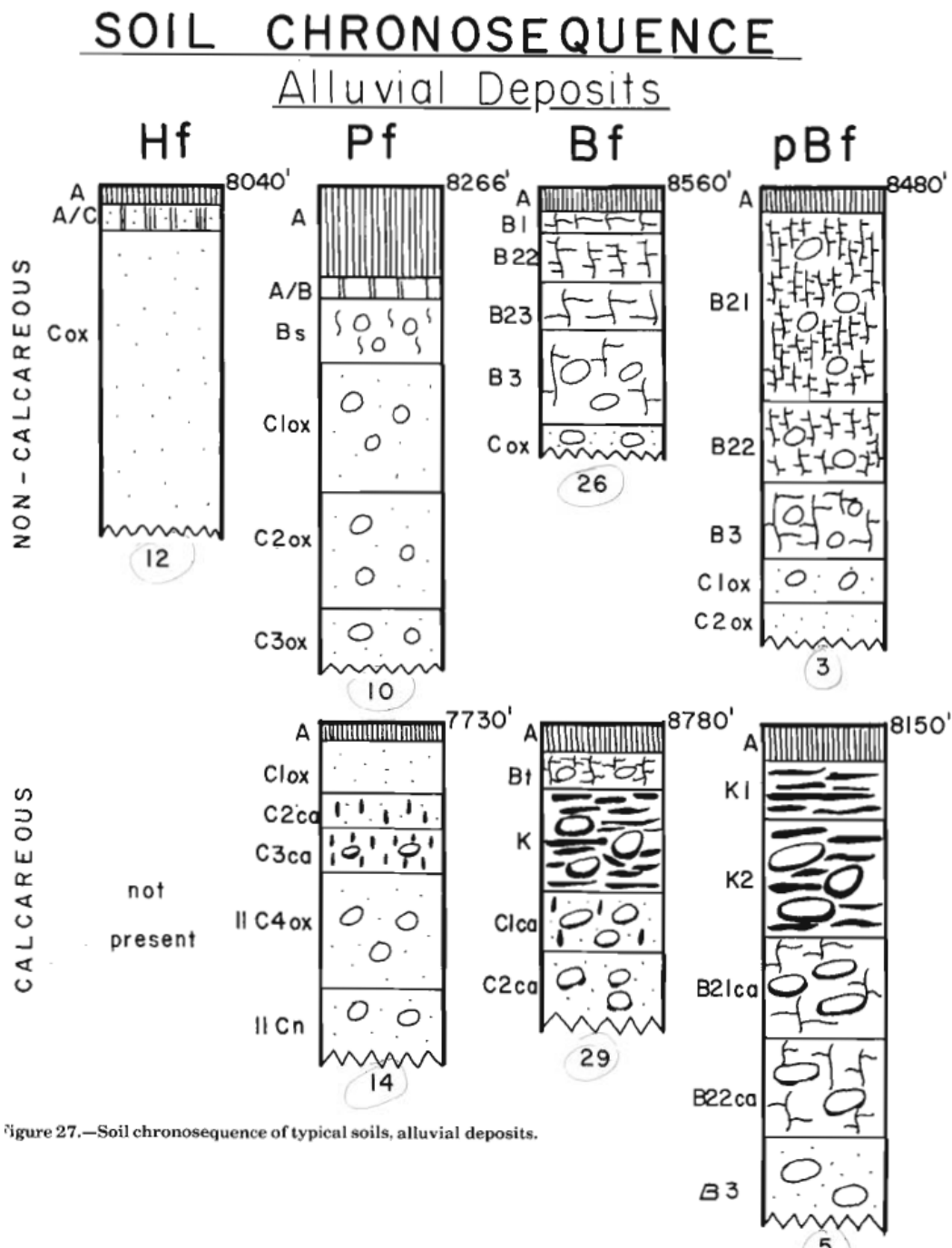


Figure 27.—Soil chronosequence of typical soils, alluvial deposits.

Fig. 4-2. Graphic representation of soil profiles on four different ages of alluvial fans (Hf, Holocene; Pf, Pinedale; Bf, Bull Lake; pBf, pre-Bull Lake). The upper non-calcareous chronosequence shows an increase of textural B horizon clay content and thickness through time. The lower calcareous chronosequence shows similar trends in pedogenic carbonate. From McCalpin, 1981.



INQUA Focus Group on Paleoseismology and Active Tectonics



paleoseismicity.org

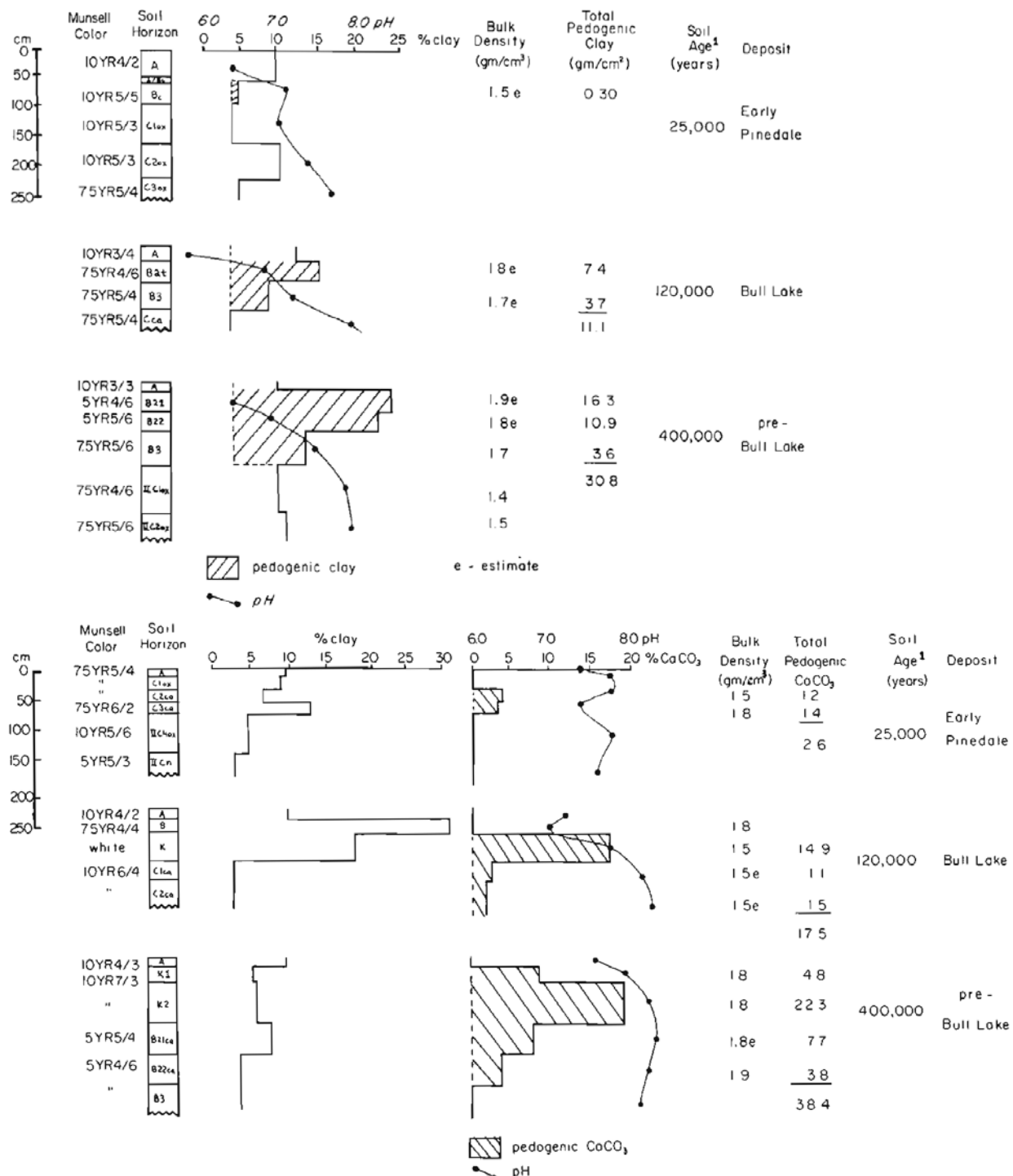


Fig. 4-3. Top half, 3 diagrams showing increase of pedogenic clay from Early Pinedale, to Bull Lake, to pre-Bull lake non-calcareous soils. Bottom half, similar diagrams for increase in pedogenic carbonate. From McCalpin, 1981.

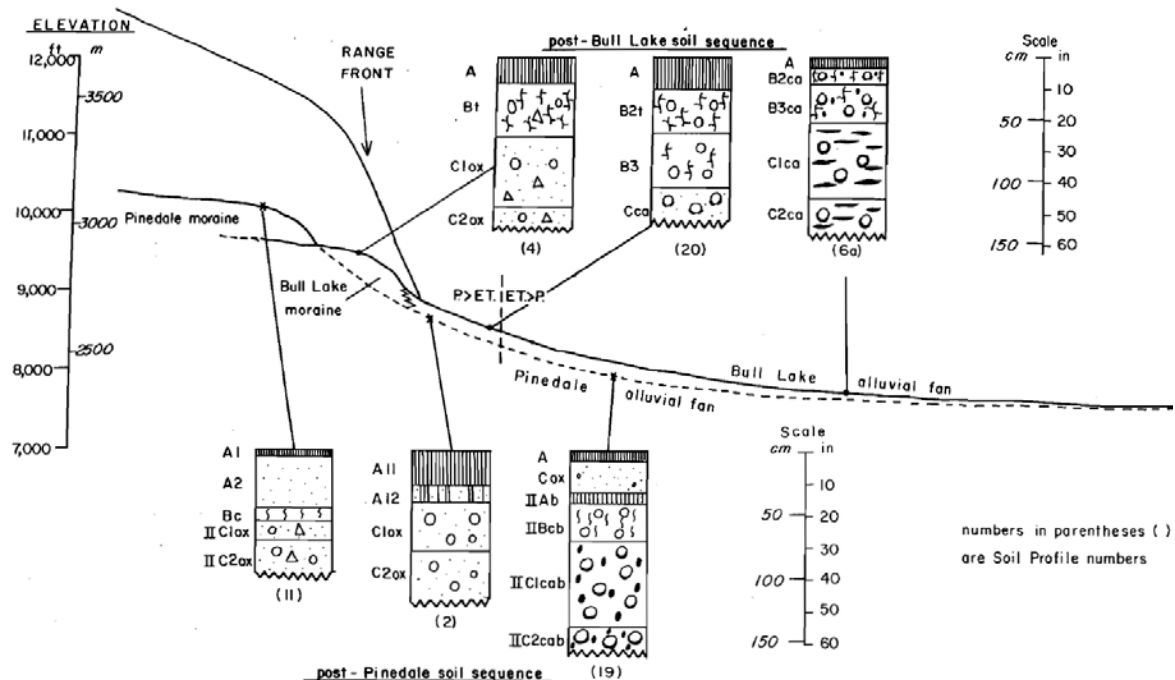


INQUA Focus Group on Paleoseismology and Active Tectonics



paleoseismicity.org

SOIL CLIMOSEQUENCES, San Luis Valley



TRENCH 3 - Fault Scarp

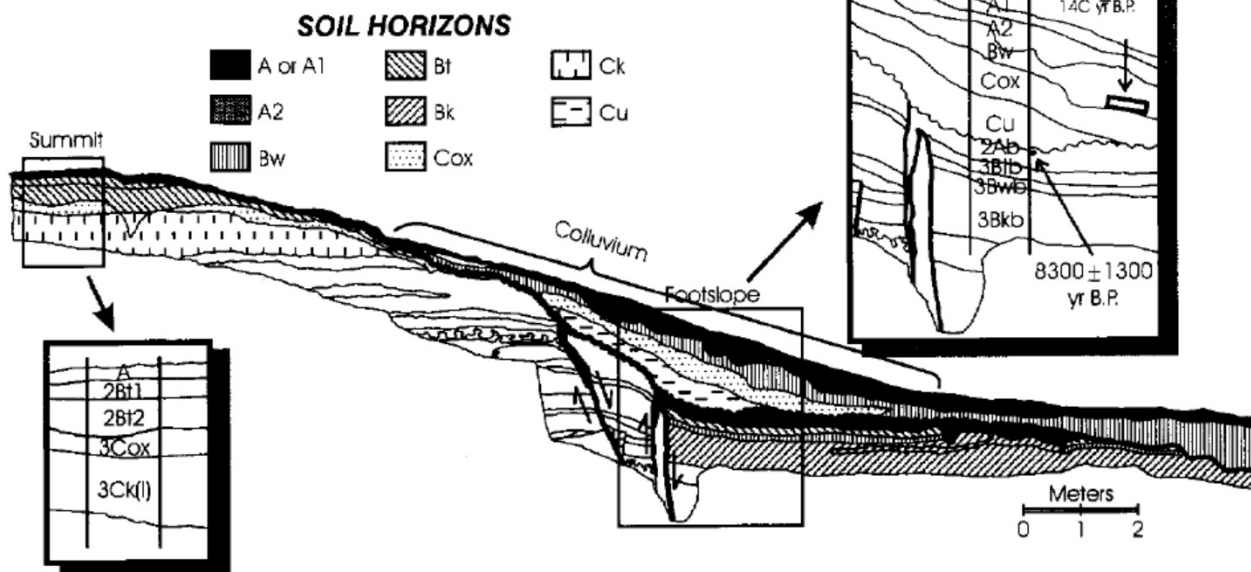


Fig. 4-4. Top half, soil climosequence for soils on Pinedale and Bull Lake deposits. From McCalpin, 1981. Bottom half, example of a soil catena (*topo-sequence*) on a fault scarp, on the Wasatch Fault, Utah. Stratigraphic units are shown by uncolored polygons. Soil profiles are weathering zones that commonly crosscut the stratigraphy created by faulting. From McCalpin and Berry, 1996.



INQUA Focus Group on Paleoseismology and Active Tectonics

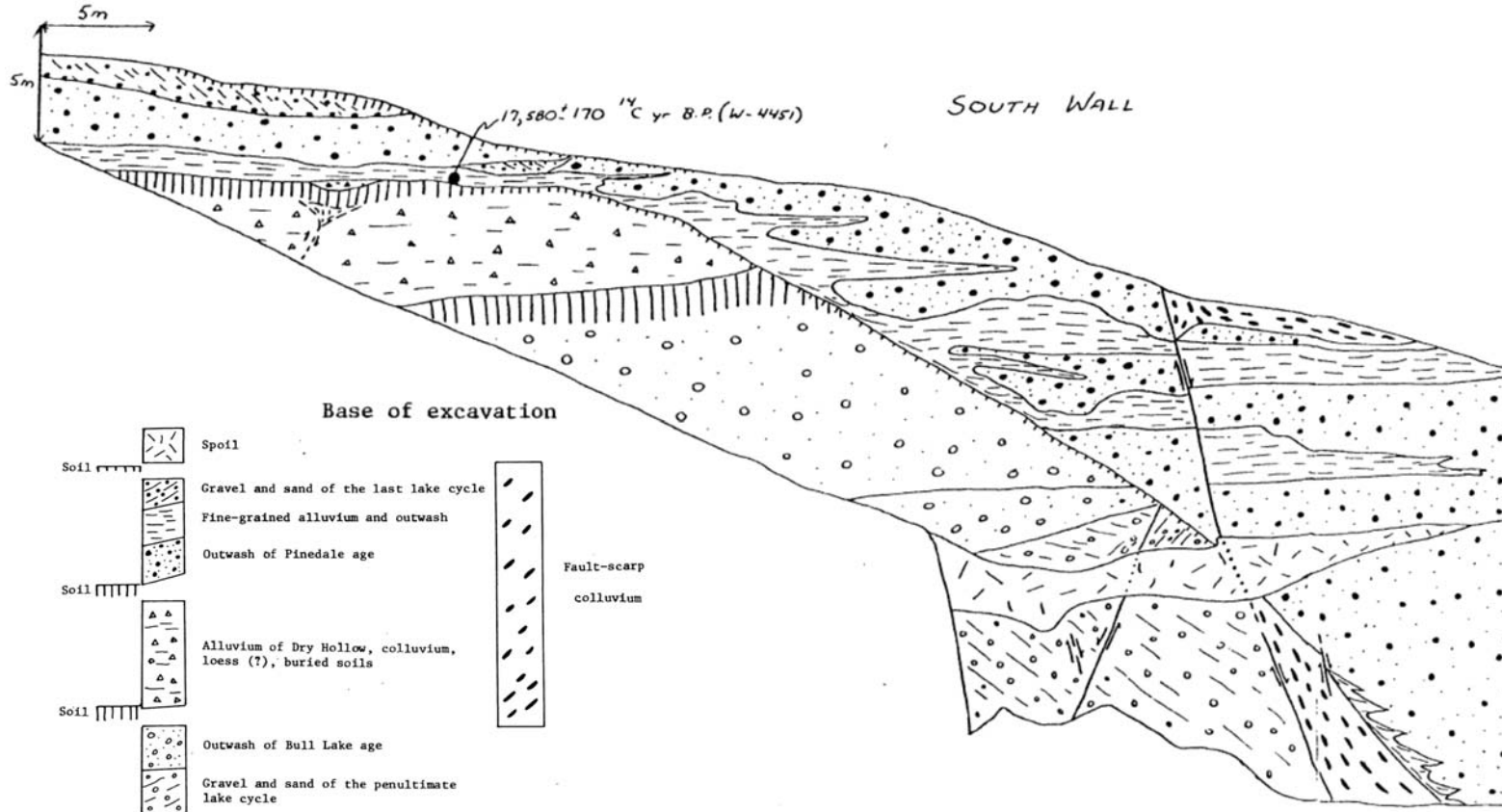


Fig. 4-5. A trench wall log that maps pedogenic soil horizons as well as stratigraphic deposits. South wall of a trench at the east end of gravel at the mouth of Big Cottonwood Canyon, Salt Lake City, UT. Trench is on the north side of road to Holladay Gun Club. Soils are indicated by closely-spaced vertical lines; the length of the lines represents soil horizon thickness and development. Four soil horizons are indicated. The oldest (lowest) is a well-developed soil on Bull Lake outwash; this soil is erosionally truncated in the center of the wall by an erosion surface that underlies Pinedale outwash. An intermediate-age soil, not as well developed as the post-Bull Lake soil, is developed on the “alluvium of Dry Hollow” which overlies the Bull Lake outwash and its paleosol. This soil is also truncated by the erosion surface. The soil is directly overlain by a C14 age of $17,580 \pm 170$ C14 yrs BP (about 20,000 cal yrs BP), which forms a close minimum age of the underlying soil. Thus, the two oldest soils developed between 20 ka and ca. 125 ka (end of the Bull Lake glaciation), and the lower soil is about twice as developed as the upper one. So neglecting time needed to deposit the outwash and fan alluvium, the lower soil took ≤ 70 ka to develop and the intermediate one took ≤ 35 ka.



INQUA Focus Group on Paleoseismology and Active Tectonics



paleoseismicity.org

There is a weak soil developed on the erosion surface, indicating a hiatus before the deposition of the Pinedale outwash. The youngest soil is at the modern ground surface at upper left, and is developed on “gravel and sand of the last lake cycle”, at ca. 15 ka. In other words, this soil represents less than 15 ka of soil development.

The neotectonic significance comes from the fact that the erosion surface faces to the right and lies upslope of the major faults, which are downthrown to the right. In the lower right corner of the wall is a wedge of “fault scarp colluvium.” Viewed in this way, the erosion surface now appears to be the upper part of a fault scarp created by post-Bull Lake (and post Dry Hollow) fault movement. The existence of the weak (<15 ka) soil developed on it suggests that the upper scarp face was stable enough for a soil to form on it, prior to the onset of Pinedale outwash deposition. That deposition basically aggraded up against and over the top of the old fault scarp and buried it.

After deposition of Pinedale outwash the fault at right moved again, displacing the outwash beds about 2-3 m down-to-the-right.

The chronology of faulting, erosion, deposition, and soil-forming hiatuses can be approximated for this cut, even though it only contains a single numerical age-date. Most of the inferred chronology depends on: (1) correlation of certain deposits with the Bull Lake (MIS6) and Pinedale (MIS2) glaciations, and (2) identifying soil horizons and estimating the time required for their development. Without the horizon soil information, the story would not be as clear.

With the development of luminescence dating, it may now be possible to directly date the finer-grained facies in this exposure to refine the chronologic story. However, interpreting luminescence dates from rapidly-deposited facies such as glacial outwash and alluvial fan debris flows, or from subaqueous facies such as nearshore sands and gravels, still carries some uncertainty. Soil profile development may be a crude chronometer, but it is unaffected by assumptions about partial bleaching and inherited grains, that in the end may make luminescence dates even less accurate than soil development dates.

REFERENCES

Colman, S.M., McCalpin, J.P., Ostendarp, D.A. and Kirkham, R.M., 1985, Map showing upper Cenozoic rocks and deposits and Quaternary faults, Rio Grande Rift, south-central Colorado: USGS Misc. Geol. Invest. Map I-1594, 2 sheets, scale 1:125,000.

Grauch, V.J.S. and Hudson, M., 2007, Guides to understanding the aeromagnetic expression of faults in sedimentary basins: Lessons learned from the central Rio Grande rift, New Mexico: *Geosphere*; December 2007; v. 3; no. 6; p. 596–623; doi: 10.1130/GES00128.

Grauch, V.J.S. and Ruleman, C.A., 2013, Identifying buried segments of active faults in the Northern Rio Grande Rift using aeromagnetic, LiDAR, and gravity data, south-central Colorado, USA: *International Journal of Geophysics*, Vol. 2013, Article ID 804216, 26 pages <http://dx.doi.org/10.1155/2013/804216>.

McCalpin, J.P., 1981, Quaternary geology and neotectonics of the west flank of the Northern Sangre de Cristo Mountains, South-Central Colorado: PhD dissertation, T-1981, Colorado School of Mines, Golden, CO, Dec. 1981, 3xx p.

McCalpin, J.P. (ed.), 2009, *Paleoseismology*, 2nd Edition: Academic Press, Elsevier Publishing, New York, 608 p.



INQUA Focus Group on Paleoseismology and Active Tectonics



paleoseismicity.org

McCalpin, J.P. and Berry, M.E., 1996, Soil catenas to estimate ages of movements on normal fault scarps, with an example from the Wasatch fault zone, Utah, USA: Catena 27:265-286.

McCalpin, J.P. and Harrison, J.B.J., 2001, Paleoseismicity of Quaternary faults near Albuquerque, New Mexico: unpublished Final Technical Report submitted to U.S. Geological Survey by GEO-HAZ Consulting, Inc., Contract 99HQGR0056, Aug. 4, 2001, 58 p.
(https://works.bepress.com/james_mccalpin/14/)

Scott, W.E., 1981, Field-trip guide to the Quaternary stratigraphy and faulting in the area north of the mouth of Big Cottonwood Canyon, Salt Lake County, Utah: US Geol. Surv., Open-File Report 81-773, 12 p.

Štěpančíková P., Dohnal J., Pánek T., Łoj M., Smolková V., Šilhán K., 2011, The application of electrical resistivity tomography and gravimetric survey as useful tools in an active tectonics study of the Sudetic Marginal Fault (Bohemian Massif, central Europe). Journal of Applied Geophysics, v. 74, p. 69-80.